



This is a repository copy of *Cerebrovascular endothelial cells form transient Notch-dependent cystic structures in zebrafish*.

White Rose Research Online URL for this paper:
<http://eprints.whiterose.ac.uk/148602/>

Version: Accepted Version

Article:

Kugler, E.C. orcid.org/0000-0003-2536-6140, van Lessen, M., Daetwyler, S. et al. (10 more authors) (2019) Cerebrovascular endothelial cells form transient Notch-dependent cystic structures in zebrafish. *EMBO Reports*. e47047. ISSN 1469-221X

10.15252/embr.201847047

© 2019 The Authors. This is an author-produced version of a paper subsequently published in *EMBO Reports*. Uploaded in accordance with the publisher's self-archiving policy.

Reuse

Items deposited in White Rose Research Online are protected by copyright, with all rights reserved unless indicated otherwise. They may be downloaded and/or printed for private study, or other acts as permitted by national copyright laws. The publisher or other rights holders may allow further reproduction and re-use of the full text version. This is indicated by the licence information on the White Rose Research Online record for the item.

Takedown

If you consider content in White Rose Research Online to be in breach of UK law, please notify us by emailing eprints@whiterose.ac.uk including the URL of the record and the reason for the withdrawal request.

Cerebrovascular endothelial cells form transient Notch-dependent cystic structures in zebrafish

Elisabeth C. Kugler * ^{1,2}, Max van Lessen ³, Stephan Daetwyler ⁴, Karishma Chhabria ^{1,2}, Aaron M. Savage ^{1,2}, Vishmi Silva ^{1,2}, Karen Plant ^{1,2}, Ryan B. MacDonald ^{1,2}, Jan Huisken ^{4,5}, Robert N. Wilkinson ^{1,2}, Stefan Schulte-Merker ³, Paul Armitage ^{1, #}, Timothy J.A. Chico * ^{1,2, #}

1 Department of Infection, Immunity and Cardiovascular Disease, University of Sheffield, Medical School, Beech Hill Road, Sheffield, S10 2RX United Kingdom.

2 The Bateson Centre, Firth Court, University of Sheffield, Western Bank, Sheffield, S10 2TN United Kingdom.

3 WWU Münster, Faculty of Medicine, Institute for Cardiovascular Organogenesis and Regeneration, Mendelstrasse 7, 48149 Münster, Germany.

4 Max Planck Institute of Molecular Cell Biology and Genetics, Pfotenhauerstrasse 108, 01307 Dresden, Germany.

5 Morgridge Institute for Research, 330 N Orchard St, Madison, WI 53715, USA.

Final Character Count (without references (12,964) and Material and Methods (9680)):

47,174

*Joint Corresponding Authors

#Joint Senior Authors

Email for correspondence: ekugler1@sheffield.ac.uk or t.j.chico@sheffield.ac.uk

Data are available on request.

Running title: Endothelial “kugeln”

Keywords: angiogenesis / endothelial cell / Notch / zebrafish / VEGF/ Wnt

Abstract

We identify a novel endothelial membrane behaviour in transgenic zebrafish. Cerebral blood vessels extrude large transient spherical structures that persist for an average of 23 minutes before regressing into the parent vessel. We term these structures “kugeln”, after the German for sphere.

Kugeln are only observed arising from the cerebral vessels and are present as late as 28 days post fertilisation. Kugeln do not communicate with the vessel lumen and can form in the absence of blood flow. They contain little or no cytoplasm but the majority are highly positive for nitric oxide reactivity. Kugeln do not interact with brain lymphatic endothelial cells (BLECs) and can form in their absence, nor do they perform a scavenging role or interact with macrophages. Inhibition of actin polymerisation, myosin II, or Notch signalling reduce kugel formation, while inhibition of VEGF or Wnt dysregulation (either inhibition or activation) increase kugel formation.

Kugeln represent a novel Notch-dependent NO-containing endothelial organelle restricted to the cerebral vessels, of currently unknown function.

Introduction

Formation of mature blood vessels requires a wide range of endothelial behaviours. These include proliferation, migration, anastomosis, lumen formation, remodelling, and pruning, alongside recruitment of non-endothelial cell types such as pericytes and vascular smooth muscle cells ¹⁻⁴. Many of these processes can be studied in vitro, but in vivo models of vascular development allow observation of endothelial behaviour within a multicellular and complex physiological environment.

Because visualising real-time embryonic vascular development in mammals is technically challenging, the zebrafish has become a widely applied model of vertebrate vascular development. Their translucency enables detailed observation of cellular behaviour without invasive instrumentation in vivo ^{5,6}. An increasing array of transgenic reporter lines that drive fluorescent gene expression in vascular cells is available. Coupling these with state-of-the-art imaging techniques, such as light sheet fluorescence microscopy (LSFM), enables detailed cellular and subcellular imaging for hours or even days during embryonic development ^{7,8}. This ability to observe vascular development in more detail and for longer durations provides new insights into blood vessel formation.

Endothelial and other cells are known to form a variety of membranous vesicles ⁹. These include apoptotic bodies (1-4µm diameter), microvesicles (0.15-1µm diameter) and exosomes (40-150nm diameter) ¹⁰. There is increasing evidence that such vesicles play important roles in intracellular signalling ¹¹, and in vascular diseases such as atherosclerosis ¹². Understanding the roles of such vesicles is therefore of both biological and clinical significance.

Here we report a novel type of endothelial cell vesicle formation with characteristics that are entirely distinct from any previously described membrane behaviour. We show that endothelial cells (ECs) of the zebrafish cerebral vasculature (but not other vessels) extrude spherical structures far larger than any previously described microvesicle¹⁰, and unlike previously described vesicles never detach from the parent endothelial cell.

Due to their unknown nature and function we termed these structures kugeln (German for spheres) and we here characterise their morphology, dynamics, and sites of occurrence. We find that kugeln are membranous protrusions that do not contain either nuclei or cytoplasm. Although very different in size and behaviour to other vesicular structures, inhibition of the cytoskeletal components filamentous actin (F-actin) formation or Myosin II reduced kugeln formation, as previously shown for cellular blebs¹³. Kugeln do not interact with brain lymphatic endothelial cells (BLECs)^{14,15} or macrophages, nor do they serve as scavengers. Kugeln formation is not influenced by either increased membrane rigidity, nor osmotic pressure, which are known to impact platelet ballooning and cellular blebbing^{13,16}.

Kugel formation can proceed in the absence of blood flow. Furthermore we show that central orchestrators of vascular development such as Notch, VEGF and Wnt signalling^{17–20} all influence kugel formation.

Together, our data suggest that kugeln represent a previously undescribed EC membrane behaviour restricted to the cerebral vessels. Their function remains unknown but their existence emphasises that our understanding of the intricate processes during vascular development is far from complete.

Results

Endothelial cells of zebrafish cerebral vessels frequently develop large extruding spherical structures

We initially observed that the endothelial cells of the cerebral vessels of transgenic Tg(kdrl:HRAS-mCherry)^{s916} zebrafish expressing an endothelial membrane-tagged reporter protein²¹ displayed rounded protrusions (**Figure 1A**). Although the appearance of these on single z-slices was similar to cross-sections of lumenized vessels, three-dimensional reconstruction showed them to be spherical abluminal protrusions (**EV Movie 1**). Due to their shape and unknown nature we termed these structures kugeln, after the German for sphere (singular kugel). The mean diameter of kugeln was $10.1 \pm 0.5\mu\text{m}$ (s.e.m.) at 3dpf (**Figure 1B**) exceeding the size of previously described membrane derived vesicles¹⁰.

Mean number of kugeln per embryo was 5.55 ± 1.12 (s.e.m.) at 3dpf, and was not significantly different between 3-5dpf ($p = 0.8571$; **Figure 1C**). We were able to observe kugeln in 28dpf animals (**Figure 1D**), confirming that kugeln are present beyond embryonic stages.

To exclude the possibility that kugeln arise as a strain-specific feature of the transgenic line Tg(kdrl:HRAS-mCherry)^{s916} we imaged a different transgenic, Tg(fli1aep:CAAX-eGFP)²² which utilizes the pan-endothelial promotor fli1a⁸ and prenylation to target eGFP to the endothelial membrane. Again, kugeln were observed to arise from cerebral vessels (**Figure 1E**). We furthermore induced transient expression of the plasmid pTol2-fli1a:myr-mCherry^{23,24}, which uses the same fli1a promotor, and utilizes myristoylation to label the EC membrane. This was performed in Tg(gata1:dsRed) transgenics to enable vessel localization. Again, kugeln were observed in these embryos (**Figure 1F**), demonstrating that kugel formation was independent of the

transgenic construct used, the promotor driving its expression, and the method of membrane tagging. Therefore, we concluded that kugeln represent a physiological behaviour of the EC membrane of the cranial vasculature.

We mapped the location of kugeln on parent vessels to determine their distribution. >90% of kugeln arose from the central vessels of the cerebral vasculature (**Figure 1G**) and none from the trunk vasculature (aorta, intersegmental vessels, dorsal longitudinal anastomotic vessel or caudal vein) at the examined time-points. The specific vessels giving rise to kugeln are shown in **Figure 1H**.

Although individual kugeln were often unilateral (present left-side but not right-sided vessels, or vice versa) overall left/right distribution was not significantly different (**Figure 1H**).

Kugeln are highly dynamic transient structures

We next observed kugel behaviour over time. Time-lapse imaging revealed kugeln were both transient and highly dynamic (**Figure 2A**). Although we expected kugeln to form new vessels, interact with other ECs to anastomose, or detach from parent vessels, kugeln always either regressed back into the parent vessel or persisted to the end of imaging without separation or anastomosis.

Quantification of kugel lifespan showed that while some regressed after minutes, others persisted for hours (**Figure 2B**). Further examination showed that kugeln displayed dynamic alteration in shape and size, including shape changes, enlargement and retraction (**Figure 2C; EV Movie 2**). This dynamic behaviour was observed not only in *Tg(kdrl:HRAS-mCherry)^{s916}* animals but also in *Tg(fli1ep:CAAX-eGFP)* (**Figure EV1A,B**) and *Tg(fli1a:myr-mCherry)*, *Tg(gata1:dsRed)* (**Figure EV1C**).

Although some animals displayed no kugeln when observed at a single timepoint (**Figure 1C**), timelapse imaging showed kugeln could develop at subsequent timepoints (**Figure 2D**).

When we studied kugel shape change over time this revealed that some kugeln displayed oscillatory diameter changes with a periodicity of minutes (**Figure 2E**). No such changes were observed in parent vessels, suggesting alterations of kugel size or shape are not directly related to blood pressure or flow but related to active membrane remodelling.

Kugeln are membranous structures whose formation is dependent on the cytoskeleton

We next investigated the composition and biogenesis of kugeln. Examining double-transgenic embryos $Tg(kdr:nls-eGFP)^{zf109}$, $Tg(kdrl:HRAS-mCherry)^{s916}$ that labelled endothelial nuclei and membrane, we never observed kugeln to contain a nucleus, nuclear defragmentation or observed nuclear mitosis nearby kugeln (**Figure 3A**). This suggests kugeln do not represent an atypical form of cell proliferation, apoptosis, or angiogenic sprouting.

Analysing the double-transgenic line $Tg(fli1a:LifeAct-mClover)^{sh467}$, $Tg(kdrl:HRAS-mCherry)^{s916}$ labelling filamentous actin (F-actin) and EC membrane, we observed that F-actin co-localized with kugeln, especially at the kugel “neck” (**Figure 3B**). Time-lapse microscopy revealed this enrichment of F-actin at the kugel neck to be highly dynamic (**EV Movie 3**).

To further examine the contents of kugeln, we imaged the double-transgenic $Tg(fli1a:eGFP)^{y1}$, $Tg(kdrl:HRAS-mCherry)^{s916}$ that labels the EC cytosol and

membrane. We were unable to visualize cytosolic GFP within kugeln indicating they contain little if any cytoplasm (**Figure 3C**).

To further characterise the content inside and tissue surrounding kugeln, we examined the triple-transgenic Tg(gata1:dsRed), Tg(nbt:GCaMP3), Tg(kdrI:HRAS-mCherry)^{s916}, that labels red blood cells (RBCs), developing neurons and EC membrane. RBCs were never observed within kugeln. Examination of neurons showed an exclusion of neural tissue (**Figure 3D**), confirming kugeln displace rather than include neural tissue.

Kugel formation is reduced by F-actin or Myosin II inhibition

Since F-actin was enriched at kugel necks, we examined whether this was necessary for growth and/or maintenance of kugeln. Thus, actin polymerization was inhibited by application of Latrunculin B. This led to a significant increase of number of kugeln per embryo (**Figure 3E**; p 0.0041), but a significant decrease of kugel diameter (**Figure 3F**; p 0.0164).

The role of Myosin II was investigated by chemical inhibition by Blebbistatin treatment. This significantly reduced the number of kugeln per embryo (**Figure 3G**; p<0.0001) but did not affect kugeln diameter (**Figure 3H**; p 0.3731).

The finding that F-actin inhibition increased, while Myosin II inhibition decreased, kugel number is consistent with the effect of these manipulations on cellular blebs¹³, suggesting some shared mechanisms of kugel and bleb biogenesis.

Blood flow is not required for kugel formation, maintenance, retraction, or oscillation

To study the impact of blood flow and blood pressure we performed exsanguination by cardiac puncture to reduce blood pressure and flow to zero. Imaging the same

animals pre- and post- exsanguination showed no effect on kugel size or shape (**Figure 4A,B**) suggesting neither flow nor pressure are needed to maintain kugeln once they have formed. To confirm this, cardiac contraction was temporarily stopped by high-dose Tricaine application and time-lapses acquired. Despite absent blood flow, kugeln still developed, changed shape and retracted (**Figure 4C** and **Figure 4D**) as seen under normal blood flow conditions.

We next performed microangiography with fluorescent dextran to investigate whether kugeln were perfused by blood or communicated with the lumen of the parent vessel. No entry of dextran into kugeln was observed (**Figure 4E**), suggesting no such communication existed, at least after kugeln were formed.

Lastly, we prevented development of heart contraction by morpholino (MO) knockdown of cardiac troponin 2a (tnnt2a)²⁵⁻²⁷. This induced a significant decrease in number of kugeln per embryo (**Figure 4F**; p<0.0001).

Together, these data suggest that blood flow is not the driving mechanism of kugel formation, retraction, or oscillation; but that vessels that have never experienced flow do not form kugeln.

Altered membrane permeability or osmotic pressure do not affect kugel formation or diameter

Since DMSO increases membrane permeability²⁸ we examined whether this had an impact on kugel formation. We incubated embryos for 24h in 2.5% DMSO and found no significant difference in kugel number (**Figure EV 2A**; p 0.1596) or diameter (**Figure EV2B**; p 0.3665).

As osmotic pressure increases cellular bleb formation and platelet ballooning^{13,16}, we examined whether kugeln were altered by increased osmotic pressure. Embryos were

incubated for 24h in a 40mM glucose solution. No significant difference was found in kugel number (**Figure EV2C**; p 0.7371) or diameter (**Figure EV2D**; p 0.7060).

Lymphatic cells did not interact with kugeln

Next we investigated the relationship between kugeln and the meningeal population of lymphatic cells, brain lymphatic endothelial cells (BLECs)¹⁴. We first investigated whether BLECs interacted physically with kugeln in the double-transgenic Tg(kdrl:HRAS-mCherry)^{s916}, Tg(fli1a:Lifeact-mClover)^{sh467}, which allowed us to visualize BLECs as mClover-positive but mCherry-negative structures (**Figure 5A-C**). BLECs were observed to be at a different anatomical depth than kugeln (**Figure 5D**) and no direct interaction between BLECs and kugeln was ever observed (n=21, 4dpf embryos; 3 experimental repeats).

To examine whether lymphatics are required for kugeln formation, BLEC formation was inhibited by MO knockdown of ccbe1 (**Figure 5E**)²¹. This had no effect on either number of kugeln per embryo (**Figure 5F**), nor kugel diameter (**Figure 5G**).

These findings were confirmed by imaging the double-transgenic Tg(kdrl:HRAS-mCherry)^{s916}, Tg(flt4^{BAC}:mCitrine)^{hu7135}, which more specifically labels BLECs (**Figure EV3A**). Again, ccbe1 MO knockdown had no effect on kugel number (**Figure EV3B&C**; p 0.1472) or diameter (**Figure EV3D**; p 0.0962).

Next, we examined whether kugeln serve an uptake function, similar to BLECs¹⁴. We studied whether IgG-conjugated Alexa Fluor 674, injected into the tectum, would be taken up by kugeln. While BLECs readily took up the IgG-conjugated Alexa, this was not observed in kugeln (**Figure 5H**; 140 kugeln from 17 4dpf embryos; **Figure EV3E** 52 kugeln from five 5dpf embryos).

Macrophages do not interact with kugeln

Since macrophages interact with vessels undergoing anastomosis²⁹, we imaged the triple transgenic line Tg(fms:GAL4.VP16)ⁱ¹⁸⁶, Tg(UAS-E1b:nfsB.mCherry)ⁱ¹¹⁴⁹, Tg(kdrl:HRAS-mCherry)^{s916}, which labels both macrophages and endothelial cells with mCherry (**Figure 6A**). To distinguish the anatomical depth of kugeln and macrophages, depth-coding was performed; also, macrophages could be identified by cell shape and movement between frames of time-lapses (**Figure 6B**). We never observed direct interaction of macrophages with kugeln (**Figure 6C; EV Movie 4**; n=21 kugeln in eight 3dpf embryo), suggesting that kugeln do not directly respond to local inflammation, and/or recruitment of macrophages²⁹.

Number of kugeln is increased by VEGF inhibition and whilst kugeln contain NO, they do not require NO synthase for their formation

Due to the essential role of VEGF in angiogenesis we examined the effect of VEGF signalling inhibition on kugel formation^{17,30}. The VEGF inhibitor AV951 significantly increased the number of kugeln per embryo (**Figure 7A**; p<0.0001), without affecting kugel diameter (**Figures 7B**; p 0.7890). Since nitric oxide (NO) is induced by VEGF³¹ we incubated embryos with the vital dye DAF-FM, which fluoresces green in contact with NO^{32,33}. We found 57.76% of kugeln (118 of 205 kugeln; 22 embryos) were fluorescent, indicating high levels of NO reactivity (**Figure 7C**). To identify at which point kugeln begin to contain NO we performed time-lapse microscopy of kugel formation after DAF-FM staining and found NO-reactivity was detectable at the start of kugel formation (**Figure 7D**). Because DAF-FM can fluoresce in acidic environments even in the absence of NO³⁴, we performed Lysotracker staining, which visualises acidic cell compartments^{35,36}. Only 17.08% of kugeln were positive for Lysotracker

(**Figure 7E**; 62 of 363 kugeln; 22 embryos) suggesting that kugeln do indeed contain NO.

We examined whether nitric oxide synthase (NOS) was required for kugel formation by application of the NOS inhibitor L-NAME^{31,37}. Neither kugel number (**Figure 7F**; p 0.4870) nor diameter were significantly altered by L-NAME treatment (**Figure 7G**; p 0.4161).

Notch signalling is required for kugel formation

Having found that VEGF signalling negatively regulates kugel formation, we studied its counter-part Notch^{19,38,39}. Pharmacological inhibition of Notch signalling by DAPT significantly reduced kugel number (**Figure 8A**; p<0.0001), while not significantly affecting kugel diameter (**Figure 8B**; p 0.0832).

Because these data suggested Notch signalling was required for kugel formation, we examined expression of the Notch ligand dll4 in the double-transgenic reporter line Tg(dll4in3:eGFP), Tg(kdrl:HRAS-mCherry)^{s916}. Upon visual examination no differential dll4 levels were observed in proximity to kugeln or kugel-parent-vessels (**Figure 8C**), suggesting that dll4 was not locally up- or down-regulated nearby kugeln.

To further examine Notch signalling, we utilized the transgenic Tg(TP1bglob:VenusPest)^{s940}, Tg(kdrl:HRAS-mCherry)^{s916}. Expression of VenusPest is under the control of the synthetic Notch responsive element TP1 and was found to mainly be expressed in the midbrain and to a lesser extent in the hindbrain; but, again, no differential expression was seen adjacent to kugeln, in kugeln, or in kugel-parent-vessels (**Figure 8D**).

To determine which component of the Notch pathway is required for kugeln formation we examined the effect of morpholino knockdown of the Notch ligands dll4, notch1b,

jagged-1a and jagged-1b. Knockdown of dll4 or jagged-1b did not significantly affect kugel number or diameter (**Figure EV4A,B,G,& H**). However, morpholino knockdown of notch1b significantly reduced kugeln number (**Figure EV4C**; p 0.0008), without affecting diameter (**Figure EV4D**). Conversely, jagged-1a knockdown significantly increased kugel diameter (**Figure EV4F**; p 0.0097) without affecting kugeln number (**Figure EV4E**).

Both inhibition and activation of Wnt signalling increase kugel number

Since the dorsal central cranial vessels are dependent on Wnt signalling^{20,40,41}, the impact of Wnt signalling on kugeln formation was studied. Inhibition of Wnt signalling was achieved by application of XAV-939⁴². This significantly increased number of kugeln per embryo (**Figure 8E**; p 0.0003), while not affecting kugel diameter (**Figure 8F**; p 0.4098).

Interestingly, activation of Wnt signalling by application of the GSK3 inhibitor XV which prevents β-catenin phosphorylation⁴³ also significantly increased number of kugeln per embryo (**Figure 8G**; p<0.0001), while again not affecting kugel diameter (**Figure 8H**).

Discussion

We here describe a previously unreported form of EC behaviour in zebrafish found only on the cerebral vessels. We believe that kugeln were not described previously due to their highly dynamic nature and low number per animal. Our discovery was greatly facilitated by state-of-the art light sheet microscopy that provided the required imaging speed and 3D imaging capability. Moreover, kugeln are only detectible in EC-membrane-tagged reporter lines whereas many previous studies have utilised

cytoplasmic reporter lines that we have shown do not label kugeln. However, retrospective analysis of multiple datasets generated in Sheffield, Münster and Dresden confirmed their existence in unrelated zebrafish colonies, and they were detected using three different approaches to label endothelial membrane. This, coupled with their restriction to the cerebral vessels and their regulation by known biological pathways such as actin polymerisation as well as VEGF-, Notch-, and Wnt-signalling confirms that kugeln formation is a real phenomenon.

Kugeln are reliably observed from 3dpf onwards but are not present at 32hpf (2.3dpf). The reason for this timing of onset is not presently known and may relate to a waning of VEGF signalling (which would otherwise suppress kugeln formation), increasing Notch signalling in the brain, or a required state of maturity of the cerebral vessels. However, kugeln persist as late as 28dpf, so they do not represent a purely embryonic phenomenon. Unfortunately, the increasing size and opacity of zebrafish after 28dpf have prevented us from imaging older animals or adults.

As well as representing the first description of kugeln, our manuscript has taken important steps towards understanding their biogenesis. Although kugel diameter greatly exceeds that of previously described vesicular membrane structures, kugel biogenesis shares common features with cellular blebs such as a requirement for actin polymerisation and Myosin II¹³. Despite an appearance reminiscent of vascular aneurysms, unlike these kugeln are not multicellular and their formation appears not to be driven by blood flow. Because complete absence of blood flow throughout development prevents kugeln formation we speculate that some exposure to blood

flow may be needed to establish EC properties in the cerebral vessels such as polarity, shear stress responses and lumenisation^{4,44}, to allow kugeln to form.

Although VEGF, Notch, and Wnt signalling have all been previously shown to play central roles in angiogenesis^{17,19,20,27,38,45}, they have not previously been implicated in vesicle biogenesis. We find that all three of these signalling pathways influence kugel formation. VEGF signalling inhibits, while Notch signalling is required for kugel formation. Our preliminary morpholino antisense studies suggested notch1b but not dll4 is required for kugel formation, and interestingly that perhaps jagged-1a may negatively regulate this. However, morpholinos are associated with a significant risk of off-target effects⁴⁶ and future studies using other approaches to induce loss-of-function of these genes will be revealing. For example, an examination of kugel formation in stable mutants of these genes would be interesting although it may be challenging to discriminate between the effects of their loss-of-function on general cerebrovascular development. The recent establishment of endothelial specific CRISPR interference may also be informative⁴⁷.

Our finding that the majority of kugeln contained high levels of NO was unexpected as NO is generally considered to passively diffuse from NO-producing cells and no NO-containing organelle has previously been described⁴⁸. We speculate that accumulation of NO in kugeln may serve to establish a signalling or storage hub as described for secreted molecules such as Fgf3⁴⁹. This would provide a facility to deliver large amounts of NO rapidly. It is interesting that kugeln contain NO early in their lifetime, which, when coupled with their lack of cytoplasm, suggests that perhaps their formation might be related to “inflation” with NO, although this might be expected

to be inhibited by L-NAME which we did not observe. Furthermore, most, but not all kugeln contain NO. It is possible therefore that regression of kugeln is associated with emptying of NO from the kugel, perhaps by diffusion into the tissue or lumen.

The link between VEGF, NO and kugeln is unclear; VEGF induces NO release from ECs³¹ but inhibits kugeln formation. It has been questioned whether zebrafish possess an orthologue of endothelial nitric oxide synthase (eNOS), but the balance of evidence suggests not⁵⁰. However, zebrafish do possess orthologues for inducible and neuronal NOS and it may be these isoforms that generated the NO we detected⁵¹.

Several key questions remain unanswered by our study. Why are kugeln restricted to the cerebral vessels and what is their function? We can presently only speculate, but the dependence of kugeln on Notch signalling may provide a clue. The brain is a site of marked Notch pathway activity to which the cerebral vessels are exposed, and this may explain the localisation of kugeln to these vessels. Several human genetic diseases affecting the cerebral vasculature are linked to the Notch pathway. For example, cerebral autosomal dominant arteriopathy with subcortical infarcts and leukoencephalopathy (CADASIL) is the most common monogenic form of ischaemic stroke and is caused by mutations in the Notch receptor NOTCH⁵²⁻⁵⁴. Cerebral cavernous malformations (CCMs) are common large vascular cavernomas due to enlarged brain sinusoids. CCMs are caused by mutations in the CCM genes, which form a complex involved in stabilisation of endothelial junctions and VEGF signalling^{55,56}. Silencing CCM genes reduces Notch signalling, again implicating Notch dysregulation with human genetic cerebrovascular diseases. Since Notch inhibition impairs kugel formation, in addition to the fact that kugeln occurs in physiologically wild type (though transgenic) animals it seems most likely that kugel formation plays a

positive, though as yet unknown, function in maintaining cerebral vessels. To test this will require discovery of a method to specifically prevent kugel formation in order to test the effect on cerebrovascular function.

It remains to be seen whether kugeln exist in mammals. Given the conservation of endothelial behaviour between zebrafish and mammals, we consider this highly likely. Although they have not previously been described, our findings show it is clear that kugeln are easy to overlook, particularly on histological examination of mammalian brains, which would easily mistake kugeln for capillaries. However, now that their existence is known, the use of membrane-tagged reporters or immunostaining, coupled with a marker of perfusion would be expected to reveal whether kugeln exist in the mammalian brain.

We conclude that we have uncovered a striking subcellular phenomenon that appears restricted to cerebral vessels, emphasising that our understanding of the intricate processes during vascular development is far from complete.

Material and Methods

Zebrafish strains, handling and husbandry. Experiments performed at the University of Sheffield conformed to UK Home Office regulations and were performed under Home Office Project Licence 70/8588 held by TJAC. Experiments performed at the Max Planck Institute of Molecular Cell Biology and Genetics in Dresden and the WWU Münster Institute for Cardiovascular Organogenesis and Regeneration conformed to guidelines of the relevant German animal ethics committees.

Maintenance of adult zebrafish in all three fish facilities was conducted according to previously described husbandry standard protocols at 28°C with a 14:10 hours (h)

light:dark cycle⁵⁷. Embryos, obtained from controlled pair- or group-mating, were incubated in E3 buffer (5mM NaCl, 0.17mM KCl, 0.33mM CaCl₂, 0.33mM MgSO₄) with or without methylene blue.

The following zebrafish lines were used; Tg(kdrl:HRAS-mCherry)^{s916} labels EC membrane⁵⁸ (AB background⁵⁹; Casper background⁶⁰), Tg(gata1:dsRed) labels red blood cells (RBCs)⁶¹, Tg(fli1aep:CAAX-eGFP) labels EC membrane²² (kindly provided by Holger Gerhardt), Tg(fli1a:eGFP)^{y1} labels EC cytoplasm⁸, Tg(kdr:nls-eGFP)^{zf109} labels EC nuclei⁶², Tg(fli1a:Lifeact-mClover)^{sh467} labels endothelial filamentous actin⁴⁷, and Tg(nbt:GCaMP3) labels neurons⁶³, Tg(dll4in3:GFP) is expressed at sites of expression of the Notch delta-like ligand 4⁴⁵ (kindly provided by the De Val lab), Tg(TP1bglob:VenusPest)^{s940} labels arterial ECs⁶⁴. BLECs were studied in the double-transgenic lines Tg(kdrl:HRAS-mCherry)^{s916}, Tg(flt4^{BAC}:mCitrine)^{hu7135}⁶⁵ and Tg(kdrl:HRAS-mCherry)^{s916}, Tg(fli1a:Lifeact-mClover)^{sh467}. Macrophages were studied in Tg(fms:GAL4.VP16)ⁱ¹⁸⁶, Tg(UAS-E1b:nfsB.mCherry)^{il149}, and Tg(kdrl:HRAS-mCherry)^{s916}⁶⁶. Transient expression of Tg(fli1:myr-mCherry), labelling EC membrane^{30,31}, was achieved by injection of plasmid (50pg) with Tol2 RNA (75pg).

Image acquisition. Datasets in Sheffield were obtained using a Zeiss Z.1 light sheet microscope with a water-dipping detection-objective (Plan-Apochromat 20x/1.0 Corr nd=1.38) and a scientific complementary metal-oxide semiconductor (sCMOS) detection unit. Data were acquired with activated pivot scan, dual-sided illumination and online fusion; properties of acquired data are as follows: 0.7x zoom, 16bit image depth, 1920x1920px image size and minimum z-stack interval (approx. 0.33 x 0.33x 0.5μm). Green and red fluorophores were excited using 488nm and 561nm laser, respectively. Used filters in sequential tracks for multi-colour images were LP560 for

both and BP505-545 and LP585, respectively. Samples were embedded in 1% or 2% LMP agarose containing 200 mg/l Tricaine (MS-222, Sigma). The image acquisition chamber was filled with E3 plus Tricaine (200mg/ml) and maintained at 28°C.

Light sheet datasets in Dresden were obtained with a custom-built multidirectional SPIM (mSPIM) setup ⁶⁷. The dorsum of the embryo head was imaged every 2.5min over 2 days with dual illumination and 3 μm z-spacing. The mSPIM setup was equipped with a Coherent Sapphire 561nm laser, two Zeiss 10x/0.2 illumination objectives, an UMPlanFL N Olympus 20x/0.5 NA detection objective and an Andor iXon 885 EM-CCD camera. To cover the cerebrovascular region, several regions were imaged and later stitched using custom image processing plugins in Fiji ⁶⁸ based on the stitching tool from Stefan Preibisch ⁶⁹. Samples were mounted in fluorinated propylene ethylene (FEP) tubes according to established mounting protocols ⁷⁰. The FEP tubes were coated with 3% methyl cellulose and filled with 0.1% low-melting agarose containing 200 mg/l Tricaine to immobilize the zebrafish embryos during time-lapse imaging.

Data acquisition for the study of BLECs was performed at the University of Münster using a Leica SP8 microscope with a 40x water immersion objective (0.75x zoom) exciting with a 514 nm argon laser, 561 nm diode-pumped solid-state laser, 633 nm helium-neon and 514 / 561 / 633 beamsplitters. Properties of data acquired were as follows: 16bit image depth, 1024 x 1024px image size and 1μm minimum z-stack interval. Sample embedding was performed in 0.8% low-melting agarose with 200mg/l Tricaine.

Microangiography. Vascular perfusion was visualized as previously described ^{71,72}, using 20μg dextran tetramethylrhodamine (2,000,000 molecular weight,

ThermoFisher) at a concentration of 10mg/µL (2nl injection volume).

Exsanguination and cessation of cardiac contraction. Exsanguination was achieved by mechanical opening of the heart with forceps. Temporary cessation of cardiac contraction was induced by treatment with 3.7mM Tricaine in E3. After 20min incubation and 30-40min image acquisition, samples were placed in E3 without Tricaine until full recovery of cardiac contraction to confirm non-lethality of Tricaine exposure.

Morpholino antisense oligomer induced gene knockdown. Inhibition of induction of cardiac contraction was achieved by injection of an ATG blocking morpholino (MO) against cardiac troponin 2 (tnnt2a) at 1.58ng/embryo (Genetools, LLC; sequence 5'-CATGTTGCTCT GATCTGACACGCA-3')²⁵.

Development of BLECs was inhibited by injection of an ATG blocking MO against collagen and calcium-binding EGF-like domain 1 (ccbe1) at 5ng/embryo (Genetools, LLC; sequence 5'-CGGGTAGATCATTTCAGACACTCTG-3')⁷³.

The role of Notch signalling was investigated by injection of an ATG blocking MO against the following components: delta-like ligand 4 (dll4; 3ng; Genetools, LLC; sequence 5' - GAGAAAGGTGAGCCAAGCTGCCATG - 3')⁷⁴, jagged-1a (jag1a; 0.1ng; 5'-GTCTGTCTGTGTCTGTCGCTGTG-3'; Genetools, LLC)⁷⁴, jagged-1b (jag1b; 0.8ng; Genetools, LLC; sequence 5'- CTGAACCTCCGTCGCAGAACATGCC - 3')⁷⁴, and notch 1b (0.25ng; Genetools, LLC; sequence 5'- GTTCCTCCGGTTACCTGGCATACAG - 3')⁷⁵.

Control MO injection was performed, according to the same protocol, with final concentrations as above (5'-CCTCTTACCTCAGTTATTATA-3'; Genetools, LLC). All MO injections were conducted at one-cell-stage using phenol red as injection tracer.

Tectum injections. Possible kugel scavenging activity was examined by injection of IgG-conjugated 150kDa Alexa Fluor 674 (0.2mg/ml, ThermoFischer) into the tectum and ventricle at 3dpf, as previously described ¹⁴.

Chemical treatments. Actin polymerization was inhibited using 100nM Latrunculin B for 1h between 96-97hpf (Sigma-Aldrich) ⁷⁶.

Myosin II was inhibited using 25μM Blebbistatin (with 1% DMSO in end-solution for solubility) for 1h between 75-76hpf (Sigma) ⁷⁷.

VEGF signalling was inhibited using VEGF receptor inhibitor AV951 ⁷⁸ at 250nM for 2h from 96-98hpf (Selleckchem; S1207; Tivozanib - AVEO pharmaceuticals).

Notch signalling was inhibited using 50μM DAPT (Sigma-Aldrich) for 12h from 84-96hpf ⁷⁹.

Wnt signalling was inhibited using 10μM XAV-939 for 4h from 72-76hpf (Sigma) ⁴². Wnt signalling activation was achieved by 10μM GSK-3 inhibitor XV for 4h from 72-76hpf (Merck) ⁴³.

Control groups for the above experiments were performed using the same concentration and duration of DMSO in the active treatments.

Inhibition of nitric oxide synthase (NOS) was achieved by 0.5mM L-NAME (Sigma-Aldrich) dissolved in E3 for 18h from 3-4dpf ³¹. Controls were incubated in E3.

The impact of osmotic pressure on kugeln was studied using 40mM glucose treatment

for 24h from 72-96hpf (Sigma). Controls were incubated in E3.

The impact of cell membrane permeability on kugeln was studied by application of 2.5% (v/v) DMSO for 24h from 72-96hpf (Sigma). Controls were incubated in E3.

Vital dye staining. In vivo visualization of nitric oxide (NO) was performed using 2.5 μ M DAF-FM-DA (Molecular Probes; D23844)³² for 6h in 4dpf embryos (96-102hpf). DMSO control was performed at the same concentration and duration. To visualize acidic cellular compartments LysoTracker Green (Molecular Probes; L7526 DND-26) was applied for 5h (96-101hpf) at a concentration of 8.33 μ M in E3^{35,36}. Controls were incubated in E3.

Image analysis and representation. Images were analysed using open-source software Fiji⁶⁸. Kymographs were produced via stack reslicing to study diameter changes of kugeln over time. To visualize data, maximum intensity projections (MIP) were generated and displayed using either grey (single channel) or red/green/blue (multi-channel) colour representations. Z-stack depth coding was conducted via hyper-stack time-coding. Intensity inversion was applied, as appropriate, to give the clearest rendering of relevant structures. Time-lapse data were displayed using MIPs. 3D image reconstruction for 360-degree rotation was performed using Arivis software.

Statistical analysis. All animals with sufficient image quality to be analysed were included. Animals were randomly allocated to treatment groups. Imaging and data analysis was performed unblinded to treatment allocation since the effects of treatment were usually obvious from the appearances of the micrographs.

Normality of data was tested using D'Agostino-Pearson omnibus test. Statistical analysis of normally distributed data was performed using a One-way ANOVA to compare multiple groups or Student's t-test to compare two groups. Non-normally

distributed data were analysed with a Kruskal-Wallis test to compare multiple groups, or Mann-Whitney test to compare two groups. Diameter of kugeln is shown as average of all kugeln per embryo, unless otherwise indicated. Analysis was performed in GraphPad Prism Version 7 (GraphPad Software, La Jolla California USA). P values are indicated as follows: $p<0.05$ *, $p<0.01$ **, $p<0.001$ ***, $p<0.0001$ ****. Data represents mean and standard deviation (s.d.), if not otherwise stated. Image representation was performed using Inkscape (<https://www.inkscape.org>).

Data Availability

All data are available on request.

Acknowledgements. We thank the Bateson Centre aquarium facility for excellent zebrafish husbandry and guidance on experiments. We are grateful for the Tol2-fli1a:myr-mCherry plasmid supplied by Naoki Mochizuki. We thank Emily Noël, the Perak lab Sheffield and Henry Roehl for sharing chemical compounds. We thank Alex McGown for advice on tectum injections. This work was supported by a University of Sheffield, Department of Infection, Immunity and Cardiovascular Disease, Imaging and Modelling Node Studentship awarded to ECK, and by a DFG grant to SSM (SCHU 1228/2-2). RBM is funded by a Wellcome Trust Seed award (210152/Z/18/Z). The Zeiss Z1 LSFM was funded via British Heart Foundation Infrastructure Award IG/15/1/31328 awarded to TJAC and RNW. We are grateful to Professor Holger Gerhardt and Professor Alastair Poole for discussions and advice.

Author Contribution. Funding Acquisition, RM, JH, SSM, RW, PA and TC; Investigation, Validation and Data Curation, EK, MvL, SD, KC, AS, VS, KP; Formal Visualization and Analysis, EK; Resources, RM, JH, SSM, RW, PA and TC; Project Administration, EK, KP, PA, and TC; Writing – Original Draft, EK, and TC; Writing – Review and Editing, all authors contributed equally;

Conflict of interest statement. Authors have declared that no conflict of interest exists.

References

1. Potente, M. & Mäkinen, T. Vascular heterogeneity and specialization in development and disease. *Nat. Rev. Mol. Cell Biol.* **18**, 477–494 (2017).
2. Adair, T. H. & Montani, J.-P. *Angiogenesis*. (Morgan & Claypool Life Sciences, 2010).
3. Davis, G. E., Stratman, A. N., Sacharidou, A. & Koh, W. Molecular basis for endothelial lumen formation and tubulogenesis during vasculogenesis and angiogenic sprouting. *Int. Rev. Cell Mol. Biol.* **288**, 101–165 (2011).
4. Dimmeler, S., Haendeler, J., Rippmann, V., Nehls, M. & Zeiher, A. M. Shear stress inhibits apoptosis of human endothelial cells. *FEBS Lett.* **399**, 71–74 (1996).
5. Gut, P., Reischauer, S., Stainier, D. Y. R. & Arnaout, R. Little Fish, Big Data: Zebrafish as a Model for Cardiovascular and Metabolic Disease. *Physiol. Rev.* **97**, 889–938 (2017).
6. Chico, T. J. A., Ingham, P. W. & Crossman, D. C. Modeling Cardiovascular Disease in the Zebrafish. *Trends Cardiovasc. Med.* **18**, 150–155 (2008).
7. Huisken, J., Swoger, J., Del Bene, F., Wittbrodt, J. & Stelzer, E. H. K. Optical sectioning deep inside live embryos by selective plane illumination microscopy. *Science* **305**, 1007–1009 (2004).
8. Lawson, N. D. & Weinstein, B. M. In Vivo Imaging of Embryonic Vascular Development Using Transgenic Zebrafish. *Dev. Biol.* **248**, 307–318 (2002).
9. Paone, S., Baxter, A. A., Hulett, M. D. & Poon, I. K. H. Endothelial cell apoptosis and the role of endothelial cell-derived extracellular vesicles in the progression of atherosclerosis. *Cell. Mol. Life Sci.* (2018). doi:10.1007/s00018-018-2983-9
10. Colombo, M., Raposo, G. & Théry, C. Biogenesis, secretion, and intercellular interactions of exosomes and other extracellular vesicles. *Annu. Rev. Cell Dev. Biol.* **30**, 255–289 (2014).
11. Zamani, P., Fereydouni, N., Butler, A. E., Navashenaq, J. G. & Sahebkar, A. The therapeutic and diagnostic role of exosomes in cardiovascular diseases. *Trends Cardiovasc. Med.* (2018). doi:10.1016/j.tcm.2018.10.010

12. Bernal-Mizrachi, L. *et al.* High levels of circulating endothelial microparticles in patients with acute coronary syndromes. *Am. Heart J.* **145**, 962–970 (2003).
13. Charras, G. T., Coughlin, M., Mitchison, T. J. & Mahadevan, L. Life and Times of a Cellular Bleb. *Biophys. J.* **94**, 1836–1853 (2008).
14. van Lessen, M. *et al.* Intracellular uptake of macromolecules by brain lymphatic endothelial cells during zebrafish embryonic development. *eLife* **6**, e25932 (2017).
15. Hogan, B. M. & Schulte-Merker, S. How to Plumb a Pisces: Understanding Vascular Development and Disease Using Zebrafish Embryos. *Dev. Cell* **42**, 567–583 (2017).
16. Agbani, E. O. *et al.* Coordinated Membrane Ballooning and Procoagulant Spreading in Human PlateletsClinical Perspective. *Circulation* **132**, 1414–1424 (2015).
17. Gerhardt, H. *et al.* VEGF guides angiogenic sprouting utilizing endothelial tip cell filopodia. *J. Cell Biol.* **161**, 1163–1177 (2003).
18. Gore, A. V., Monzo, K., Cha, Y. R., Pan, W. & Weinstein, B. M. Vascular Development in the Zebrafish. *Cold Spring Harb. Perspect. Med.* **2**, (2012).
19. Siekmann, A. F. & Lawson, N. D. Notch signalling limits angiogenic cell behaviour in developing zebrafish arteries. *Nature* **445**, 781–784 (2007).
20. Parmalee, N. L. & Kitajewski, J. Wnt Signaling in Angiogenesis. *Curr. Drug Targets* **9**, 558–564 (2008).
21. Hogan, B. M. *et al.* Ccbe1 is required for embryonic lymphangiogenesis and venous sprouting. *Nat. Genet.* **41**, 396–398 (2009).
22. Gebala, V., Collins, R., Geudens, I., Phng, L.-K. & Gerhardt, H. Blood flow drives lumen formation by inverse membrane blebbing during angiogenesis in vivo. *Nat. Cell Biol.* **18**, ncb3320 (2016).
23. Kashiwada, T. *et al.* beta-catenin-dependent transcription is central to Bmp-mediated formation of venous vessels. *Development* dev.115576 (2015). doi:10.1242/dev.115576
24. Kwon, H.-B. *et al.* The parallel growth of motoneuron axons with the dorsal aorta depends on Vegfc/Vegfr3 signaling in zebrafish. *Development* **140**, 4081–4090 (2013).

25. Sehnert, A. J. *et al.* Cardiac troponin T is essential in sarcomere assembly and cardiac contractility. *Nat. Genet.* **31**, 106–110 (2002).
26. Packham, I. M. *et al.* Microarray profiling reveals CXCR4a is downregulated by blood flow in vivo and mediates collateral formation in zebrafish embryos. *Physiol. Genomics* **38**, 319–327 (2009).
27. Watson, O. *et al.* Blood flow suppresses vascular Notch signalling via dlx4 and is required for angiogenesis in response to hypoxic signalling. *Cardiovasc. Res.* **100**, 252–261 (2013).
28. Notman, R., Noro, M., O’Malley, B. & Anwar, J. Molecular basis for dimethylsulfoxide (DMSO) action on lipid membranes. *J. Am. Chem. Soc.* **128**, 13982–13983 (2006).
29. Fantin, A. *et al.* Tissue macrophages act as cellular chaperones for vascular anastomosis downstream of VEGF-mediated endothelial tip cell induction. *Blood* **116**, 829–840 (2010).
30. Tammela, T. *et al.* Blocking VEGFR-3 suppresses angiogenic sprouting and vascular network formation. *Nature* **454**, 656–660 (2008).
31. Ziche, M. *et al.* Nitric oxide synthase lies downstream from vascular endothelial growth factor-induced but not basic fibroblast growth factor-induced angiogenesis. *J. Clin. Invest.* **99**, 2625–2634 (1997).
32. Kojima, H. *et al.* Detection and imaging of nitric oxide with novel fluorescent indicators: diaminofluoresceins. *Anal. Chem.* **70**, 2446–2453 (1998).
33. Kojima, null *et al.* Fluorescent Indicators for Imaging Nitric Oxide Production. *Angew. Chem. Int. Ed Engl.* **38**, 3209–3212 (1999).
34. Zhang, X. *et al.* Interfering with Nitric Oxide Measurements 4,5-diaminofluorescein reacts with dehydroascorbic acid and ascorbic acid. *J. Biol. Chem.* **277**, 48472–48478 (2002).
35. Haller, T., Dietl, P., Deetjen, P. & Völkl, H. The lysosomal compartment as intracellular calcium store in MDCK cells: a possible involvement in InsP₃-mediated Ca²⁺ release. *Cell Calcium* **19**, 157–165 (1996).
36. Zucker, R. M., Hunter, S. & Rogers, J. M. Confocal laser scanning microscopy of apoptosis in organogenesis-stage mouse embryos. *Cytometry* **33**, 348–354 (1998).

37. Gray, C. *et al.* Ischemia is not required for arteriogenesis in zebrafish embryos. *Arterioscler. Thromb. Vasc. Biol.* **27**, 2135–2141 (2007).
38. Thomas, J.-L. *et al.* Interactions between VEGFR and Notch signaling pathways in endothelial and neural cells. *Cell. Mol. Life Sci. CMS* **70**, 1779–1792 (2013).
39. Bentley, K., Mariggi, G., Gerhardt, H. & Bates, P. A. Tipping the balance: robustness of tip cell selection, migration and fusion in angiogenesis. *PLoS Comput. Biol.* **5**, e1000549 (2009).
40. Vanhollebeke, B. *et al.* Tip cell-specific requirement for an atypical Gpr124- and Reck-dependent Wnt/beta-catenin pathway during brain angiogenesis. *eLife* **4**, (2015).
41. Hübner, K. *et al.* Wnt/beta-catenin signaling regulates VE-cadherin-mediated anastomosis of brain capillaries by counteracting S1pr1 signaling. *Nat. Commun.* **9**, 4860 (2018).
42. Huang, S.-M. A. *et al.* Tankyrase inhibition stabilizes axin and antagonizes Wnt signalling. *Nature* **461**, 614–620 (2009).
43. Du, J. *et al.* A kinesin signaling complex mediates the ability of GSK-3beta to affect mood-associated behaviors. *Proc. Natl. Acad. Sci. U. S. A.* **107**, 11573–11578 (2010).
44. Dekker, R. J. *et al.* Prolonged fluid shear stress induces a distinct set of endothelial cell genes, most specifically lung Krüppel-like factor (KLF2). *Blood* **100**, 1689–1698 (2002).
45. Sacilotto, N. *et al.* Analysis of Dll4 regulation reveals a combinatorial role for Sox and Notch in arterial development. *Proc. Natl. Acad. Sci. U. S. A.* **110**, 11893–11898 (2013).
46. Kok, F. O. *et al.* Reverse genetic screening reveals poor correlation between Morpholino-induced and mutant phenotypes in zebrafish. *Dev. Cell* **32**, 97–108 (2015).
47. Savage, A. M. *et al.* tmem33 is essential for VEGF-mediated endothelial calcium oscillations and angiogenesis. *Nat. Commun.* **10**, 732 (2019).
48. Thomas, D. D. Breathing new life into nitric oxide signaling: A brief overview of the interplay between oxygen and nitric oxide. *Redox Biol.* **5**, 225–233 (2015).
49. Durdu, S. *et al.* Luminal signalling links cell communication to tissue architecture during organogenesis. *Nature* 120–124 (2014). doi:10.1038

50. Syeda, F., Hauton, D., Young, S. & Egginton, S. How ubiquitous is endothelial NOS? *Comp. Biochem. Physiol. A. Mol. Integr. Physiol.* **166**, 207–214 (2013).
51. Lepiller, S. *et al.* Imaging of nitric oxide in a living vertebrate using a diamino-fluorescein probe. *Free Radic. Biol. Med.* **43**, 619–627 (2007).
52. Joutel, A. *et al.* Notch3 mutations in CADASIL, a hereditary adult-onset condition causing stroke and dementia. *Nature* **383**, 707–710 (1996).
53. Joutel, A. *et al.* The ectodomain of the Notch3 receptor accumulates within the cerebrovasculature of CADASIL patients. *J. Clin. Invest.* **105**, 597–605 (2000).
54. Karschnia, P., Nishimura, S. & Louvi, A. Cerebrovascular disorders associated with genetic lesions. *Cell. Mol. Life Sci. CMLS* **76**, 283–300 (2019).
55. Renz, M. *et al.* Regulation of β1 integrin-Klf2-mediated angiogenesis by CCM proteins. *Dev. Cell* **32**, 181–190 (2015).
56. You, C. *et al.* Loss of CCM3 impairs DLL4-Notch signalling: implication in endothelial angiogenesis and in inherited cerebral cavernous malformations. *J. Cell. Mol. Med.* **17**, 407–418 (2013).
57. Westerfield, M. *The Zebrafish Book: A Guide for Laboratory use of Zebrafish (Brachydanio rerio)*. (University of Oregon Press, 1993).
58. Chi, N. C. *et al.* Foxn4 directly regulates tbx2b expression and atrioventricular canal formation. *Genes Dev.* **22**, 734–739 (2008).
59. Streisinger, G., Walker, C., Dower, N., Knauber, D. & Singer, F. Production of homozygous diploid zebra fish (*Brachydanio rerio*). *Nature* **291**, 293–6 (1981).
60. White, R. M. *et al.* Transparent Adult Zebrafish as a Tool for In Vivo Transplantation Analysis. *Cell Stem Cell* **2**, 183–189 (2008).
61. Traver, D. *et al.* Transplantation and in vivo imaging of multilineage engraftment in zebrafish bloodless mutants. *Nat Immunol* **4**, 1238–1246 (2003).
62. Blum, Y. *et al.* Complex cell rearrangements during intersegmental vessel sprouting and vessel fusion in the zebrafish embryo. *Dev. Biol.* **316**, 312–322 (2008).

63. Bergmann, K. *et al.* Imaging Neuronal Activity in the Optic Tectum of Late Stage Larval Zebrafish. *J. Dev. Biol.* **6**, 6 (2018).
64. Ninov, N., Borius, M. & Stainier, D. Y. R. Different levels of Notch signaling regulate quiescence, renewal and differentiation in pancreatic endocrine progenitors. *Dev. Camb. Engl.* **139**, 1557–1567 (2012).
65. Impel, A. van *et al.* Divergence of zebrafish and mouse lymphatic cell fate specification pathways. *Development* **141**, 1228–1238 (2014).
66. Gray, C. *et al.* Simultaneous intravital imaging of macrophage and neutrophil behaviour during inflammation using a novel transgenic zebrafish. *Thromb. Haemost.* **105**, 811–819 (2011).
67. Huisken, J. & Stainier, D. Y. R. Even fluorescence excitation by multidirectional selective plane illumination microscopy (mSPIM). *Opt. Lett.* **32**, 2608–2610 (2007).
68. Schindelin, J. *et al.* Fiji - an Open Source platform for biological image analysis. *Nat. Methods* **9**, (2012).
69. Preibisch, S., Saalfeld, S. & Tomancak, P. Globally optimal stitching of tiled 3D microscopic image acquisitions. *Bioinformatics* **25**, 1463–1465 (2009).
70. Kaufmann, A., Mickoleit, M., Weber, M. & Huisken, J. Multilayer mounting enables long-term imaging of zebrafish development in a light sheet microscope. *Dev. Camb. Engl.* **139**, 3242–3247 (2012).
71. Schmitt, C. E., Holland, M. B. & Jin, S.-W. Visualizing vascular networks in zebrafish: an introduction to microangiography. *Methods Mol. Biol. Clifton NJ* **843**, 59–67 (2012).
72. Weinstein, B. M., Stemple, D. L., Driever, W. & Fishman, M. C. Gridlock, a localized heritable vascular patterning defect in the zebrafish. *Nat. Med.* **1**, 1143–1147 (1995).
73. Guen, L. L. *et al.* Ccbe1 regulates Vegfc-mediated induction of Vegfr3 signaling during embryonic lymphangiogenesis. *Development* **141**, 1239–1249 (2014).
74. Geudens, I. *et al.* Role of delta-like-4/Notch in the formation and wiring of the lymphatic network in zebrafish. *Arterioscler. Thromb. Vasc. Biol.* **30**, 1695–1702 (2010).

75. Quillien, A. *et al.* Distinct Notch signaling outputs pattern the developing arterial system. *Dev. Camb. Engl.* **141**, 1544–1552 (2014).
76. Morton, W. M., Ayscough, K. R. & McLaughlin, P. J. Latrunculin alters the actin-monomer subunit interface to prevent polymerization. *Nat. Cell Biol.* **2**, 376–378 (2000).
77. Kovács, M., Tóth, J., Hetényi, C., Málnási-Csizmadia, A. & Sellers, J. R. Mechanism of blebbistatin inhibition of myosin II. *J. Biol. Chem.* **279**, 35557–35563 (2004).
78. Nakamura, K. *et al.* KRN951, a highly potent inhibitor of vascular endothelial growth factor receptor tyrosine kinases, has antitumor activities and affects functional vascular properties. *Cancer Res.* **66**, 9134–9142 (2006).
79. Geling, A., Steiner, H., Willem, M., Bally-Cuif, L. & Haass, C. A gamma-secretase inhibitor blocks Notch signaling in vivo and causes a severe neurogenic phenotype in zebrafish. *EMBO Rep.* **3**, 688–694 (2002).

Figure Legends

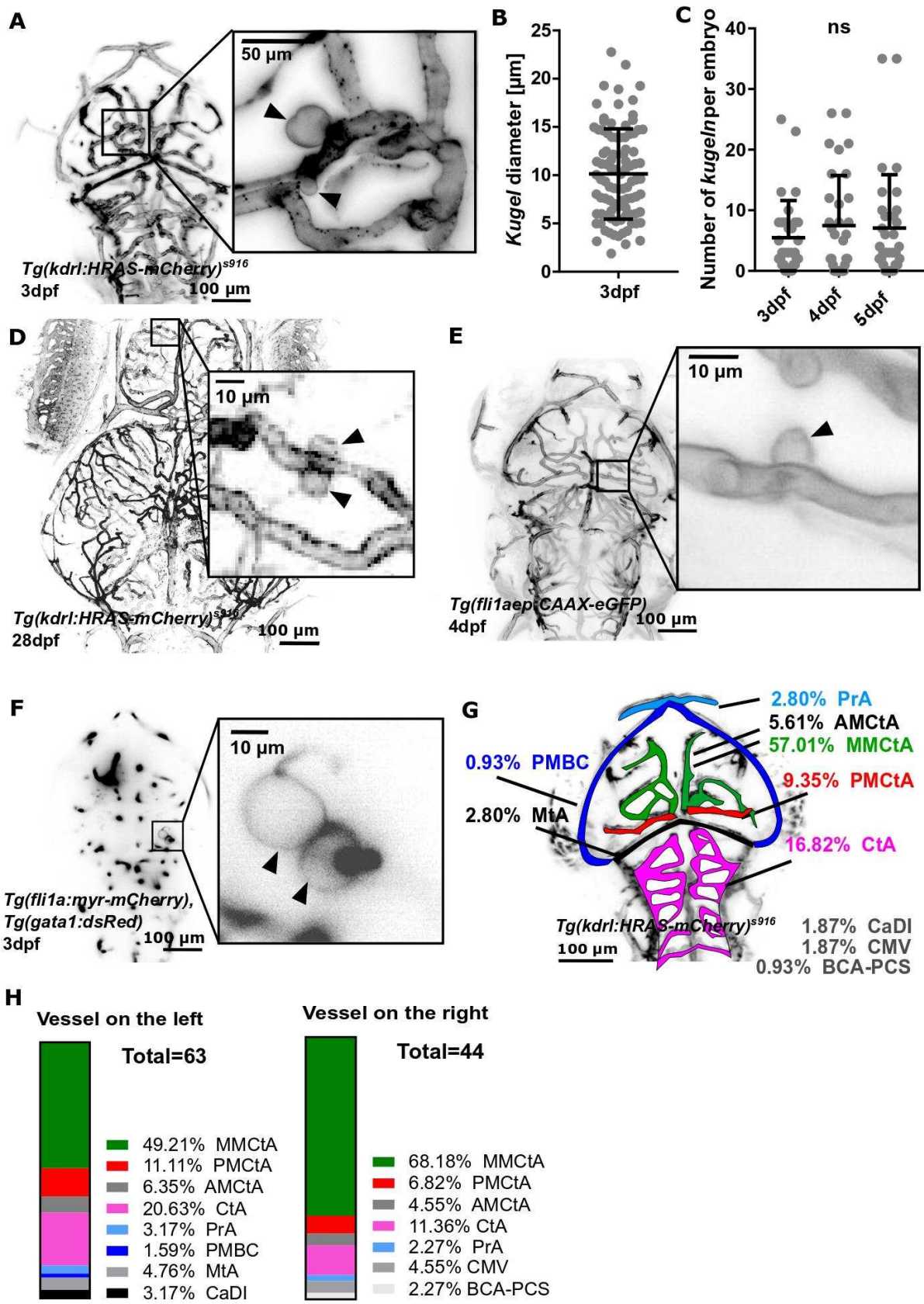


Figure 1| Endothelial cells of the zebrafish embryonic cerebral vessels develop “kugeln”; large spherical membrane protrusions.

A MIP of cerebral vessels of 3dpf Tg(kdrl:HRAS-mCherry)^{s916} embryo (grey LUT; inverted). Higher magnification panel showing two kugeln (arrowheads) arising from the middle mesencephalic central artery (MM CtA).

B Diameter of kugeln at 3dpf (mean \pm s.e.m. 10.13 ± 0.49 ; n=93 kugeln from 32 3dpf embryos; 3 experimental repeats).

C Number of kugeln per embryo in 3, 4 and 5dpf animals was not statistically significantly different (mean \pm s.e.m. 3dpf 5.47 ± 1.09 , 4dpf 7.47 ± 1.46 , 5dpf 7.09 ± 1.55 ; p = 0.8571; 3dpf: 175 kugeln from 32 embryos; 4dpf: 239 kugeln from 32 embryos, 5dpf: 227 kugeln from 32 embryos; 4 experimental repeats; Kruskal-Wallis test).

D Kugeln (arrowheads) could be observed in 28dpf animals.

E MIP of cerebral vessels of 4dpf Tg(fli1aep:CAAX-eGFP) embryo (grey LUT; inverted). Higher magnification panel shows a kugel (arrowhead) protruding from the posterior mesencephalic central artery (PM CtA).

F Single Z-plane micrograph of cerebral vessels of a 3dpf Tg(gata1:dsRed), injected with a Tol2-fli1a:myr-Cherry construct showing two kugeln (arrowheads) in the higher magnification panel protruding from the MM CtA.

G Locations and proportion of kugeln on cerebral vessels (colour coded by vessel; total n=107 kugeln from 34 4dpf embryos; 3 experimental repeats). AM CtA – anterior mesencephalic central artery, BCA – basal communicating artery, CaDI – caudal division of internal carotid artery, CMV – communicating vessel, CtA – central arteries, MM CtA – middle mesencephalic central artery, MtA – metencephalic artery, PCS –

posterior communicating segment, PMBC – posterior midbrain channel, PMCtA – posterior mesencephalic central artery, PrA – prosencephalic artery.

H Location of kugeln by vessel and laterality (107 kugeln from 34 4dpf embryos; 3 experimental repeats comparison of left vs right p 0.3592; Mann-Whitney U test).

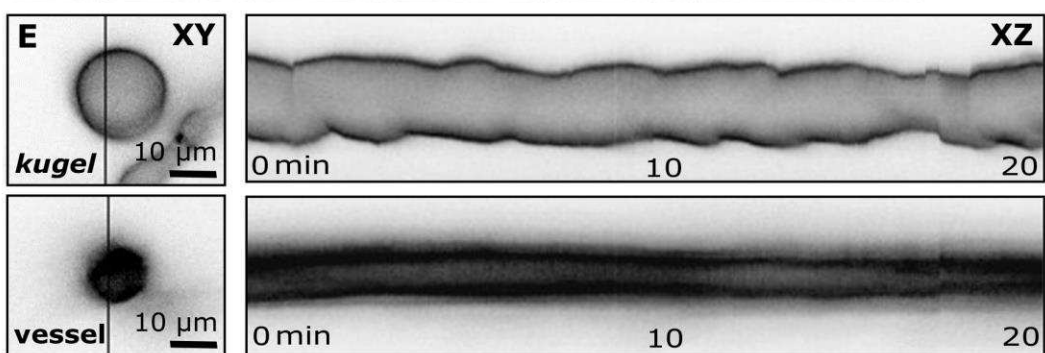
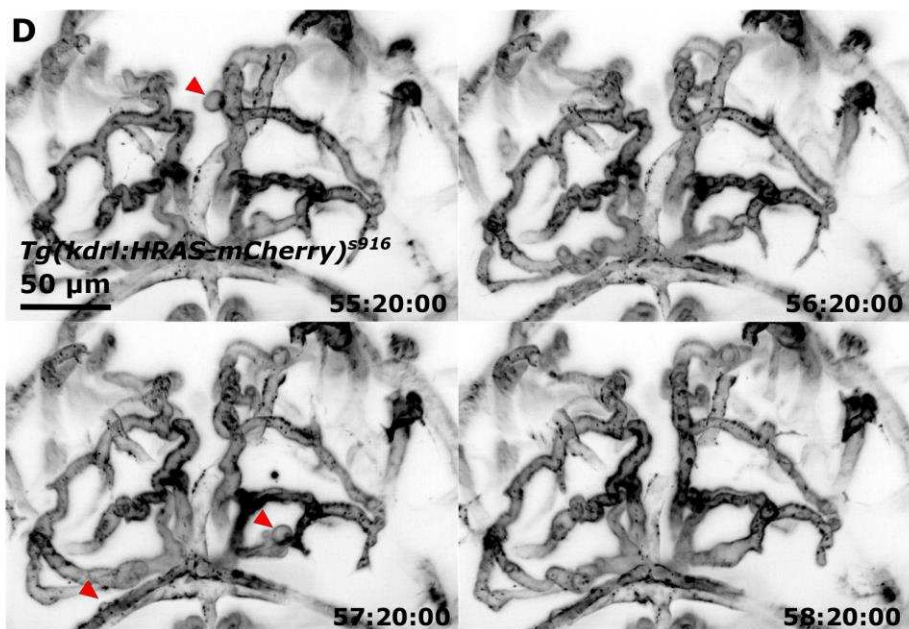
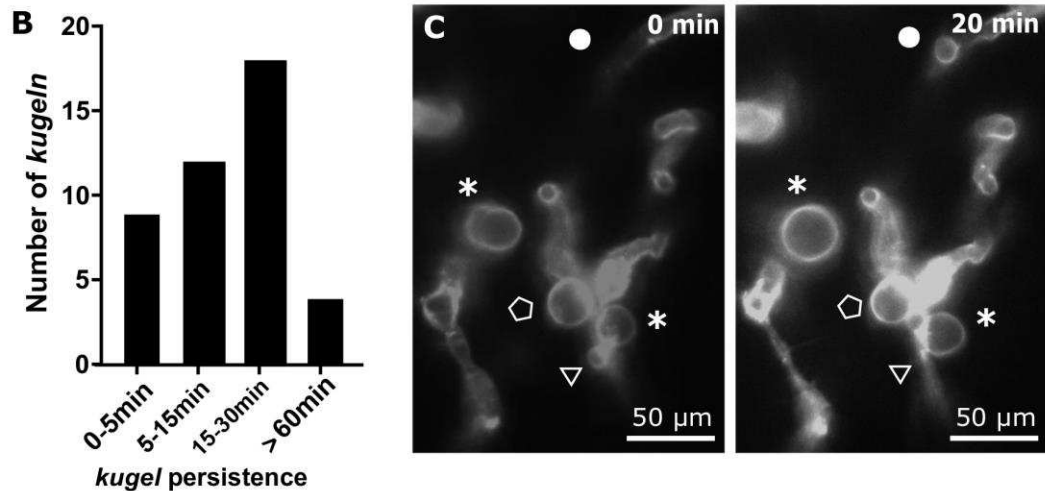
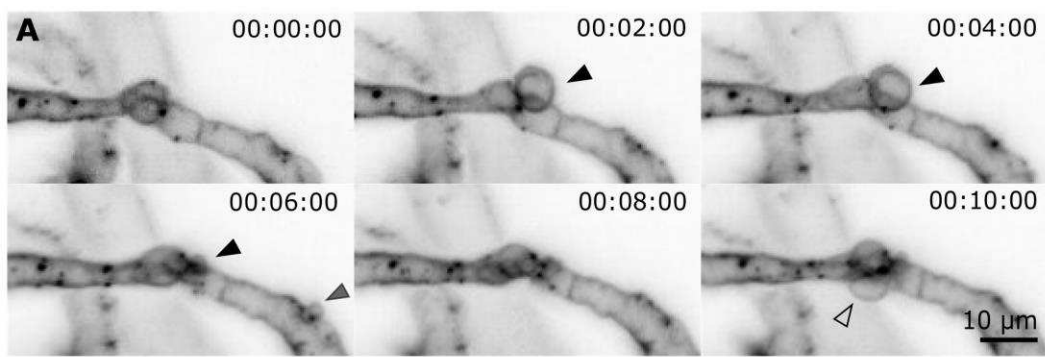


Figure 2| Endothelial kugeln are transient and dynamically alter shape and size.

A MIPs of a time-series light sheet acquisition shows three different kugeln (kugel 1 – black arrowhead; kugel 2 – grey arrowhead; kugel 3 – unfilled arrowhead) protruding and retracting from parent vessels (2min intervals; inverted LUT).

B Kugeln persisted for variable durations before regression into the parent vessel (43 kugeln from 9 4dpf embryos; 4 experimental repeats).

C MIPs taken 20min apart showing examples of different kugel behaviour including shape changes (asterisk), expansion (circle), retraction (triangle), or little change (pentagon).

D MIPs taken 1h apart show that kugeln may be observed at one time-point (red arrowhead, 55:20:00) but not 1h later in the same animal (56:20:00) and to develop on other vessels 1h later (57:20:00) which again have regressed by 58:20:00.

E Kymographs generated by line-scanning across the diameter of a typical kugel shows that kugel diameter oscillated with a periodicity of minutes, while no such oscillations were observed in adjacent similarly sized cerebral vessels (all images grey LUT; inverted).

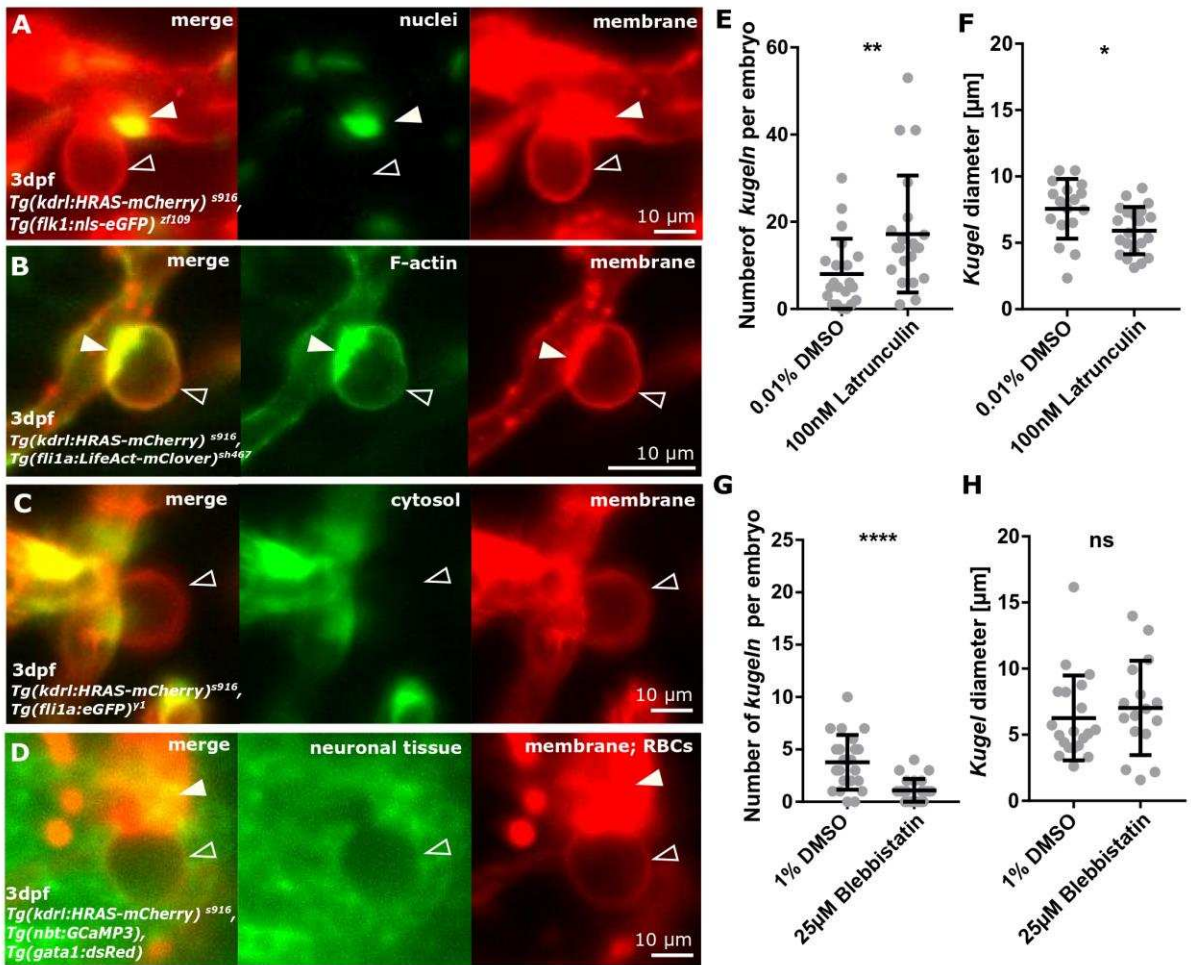


Figure 3| Endothelial kugeln are non-nucleated with a filamentous actin-enriched neck.

A Double transgenic visualizing endothelial membrane (red) and endothelial nuclei (green). Endothelial nuclei (arrowhead) were observed close to but never within the kugel (unfilled arrowhead).

B Double transgenic showing endothelial membrane (red) and endothelial F-actin (green). F-actin was found to localize at the neck of the kugeln (arrowhead; see also: EV Movie3).

C Double transgenic showing endothelial membrane (red) and endothelial cytoplasm (green). The cytoplasmic reporter was visible in the parent vessel but not in the kugel (unfilled arrowhead).

- D** Triple transgenic showing endothelial membrane (red), neurons (green) and erythrocytes (red). Surrounding neurons were excluded from the volume of the kugel (unfilled arrowhead) and erythrocytes were not observed inside kugeln (arrowhead).
- E** Treatment with the inhibitor of actin polymerization Latrunculin B statistically significantly increased number of kugeln per embryo (100nM 1 hour; **p = 0.0041; control n=21 embryos 8.05 ± 1.76 (mean \pm s.e.m.); Latrunculin n=21 embryos 17.19 ± 2.93 (mean \pm s.e.m.); 4dpf; 3 experimental repeats; Mann-Whitney U test).
- F** Latrunculin B treatment statistically significantly reduced kugel diameter (*p = 0.0164; control n=169 kugeln from 21 embryos 7.56 ± 2.25 (mean \pm s.e.m.); Latrunculin n=361 kugeln from 21 embryos 5.91 ± 1.78 (mean \pm s.e.m.); 4dpf; 3 experimental repeats; Student's t-test).
- G** Treatment with the Myosin II inhibitor Blebbistatin statistically significantly reduced number of kugeln per embryo (25 μ M 1h; ****p <0.0001; control n=22 embryos 3.77 ± 0.56 (mean \pm s.e.m.), Blebbistatin n=24 embryos 1.08 ± 0.22 (mean \pm s.e.m.); 3dpf; 3 experimental repeats; Mann-Whitney U test).
- H** Blebbistatin treatment had no effect on kugel diameter (p = 0.3731; control n=83 kugeln from 22 embryos 6.27 ± 0.72 (mean \pm s.e.m.), Blebbistatin n=26 kugeln from 24 embryos 7.02 ± 0.89 (mean \pm s.e.m.); 3dpf; 3 experimental repeats; Mann-Whitney U test).

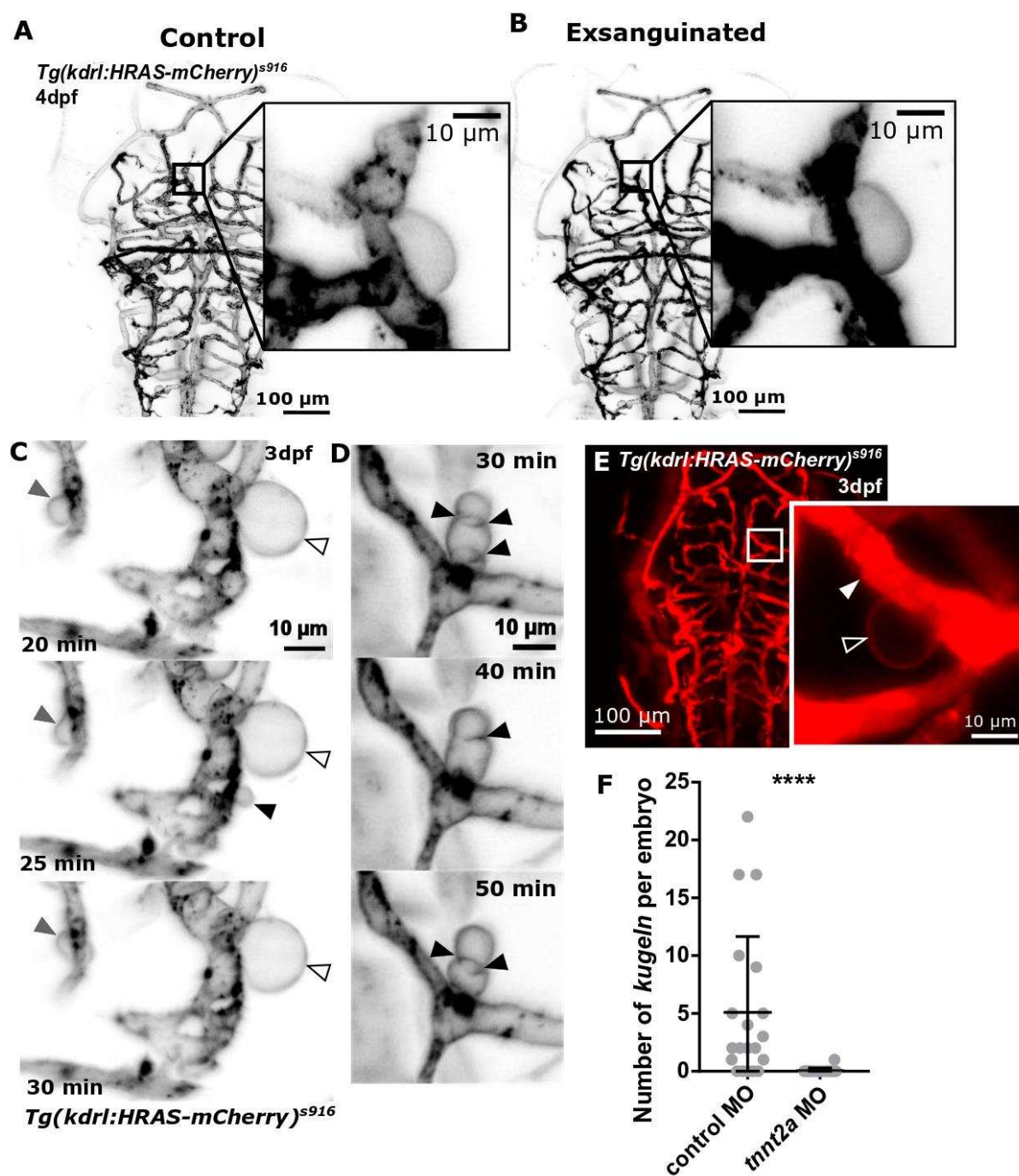


Figure 4 | The relationship between endothelial kugeln and blood flow

A MIP of the cerebral vessels of a 4dpf embryo before exsanguination (grey LUT; inverted).

B MIP of the same embryo after exsanguination, which did not alter kugeln size.

C Time-lapse imaging of an embryo with transiently halted cardiac contraction (using Tricaine). Despite absent blood flow kugeln still changed shape (grey arrowhead),

retained shape (white arrowhead) or protruded and retracted (black arrowhead; time post cessation of flow is indicated on micrographs; 3dpf; grey inverted LUT).

D Time-lapse of an embryo with transiently halted cardiac contraction as in (C) showed that kugel diameter still oscillates (time post cessation of flow).

E Dextran microangiography filled perfused vessels with dextran (arrowhead), while dextran was not observed to enter kugeln (unfilled arrowhead).

F Inhibition of cardiac contraction by tnnt2a morpholino (MO) knockdown statistically significantly reduced kugel number per embryo (**** $p<0.0001$; control n=20 embryos 5.10 \pm 1.47 (mean \pm s.e.m.), tnnt2a MO=18 embryos 0.06 \pm 0.06 (mean \pm s.e.m.); 3dpf; 3 experimental repeats; Mann-Whitney U test).

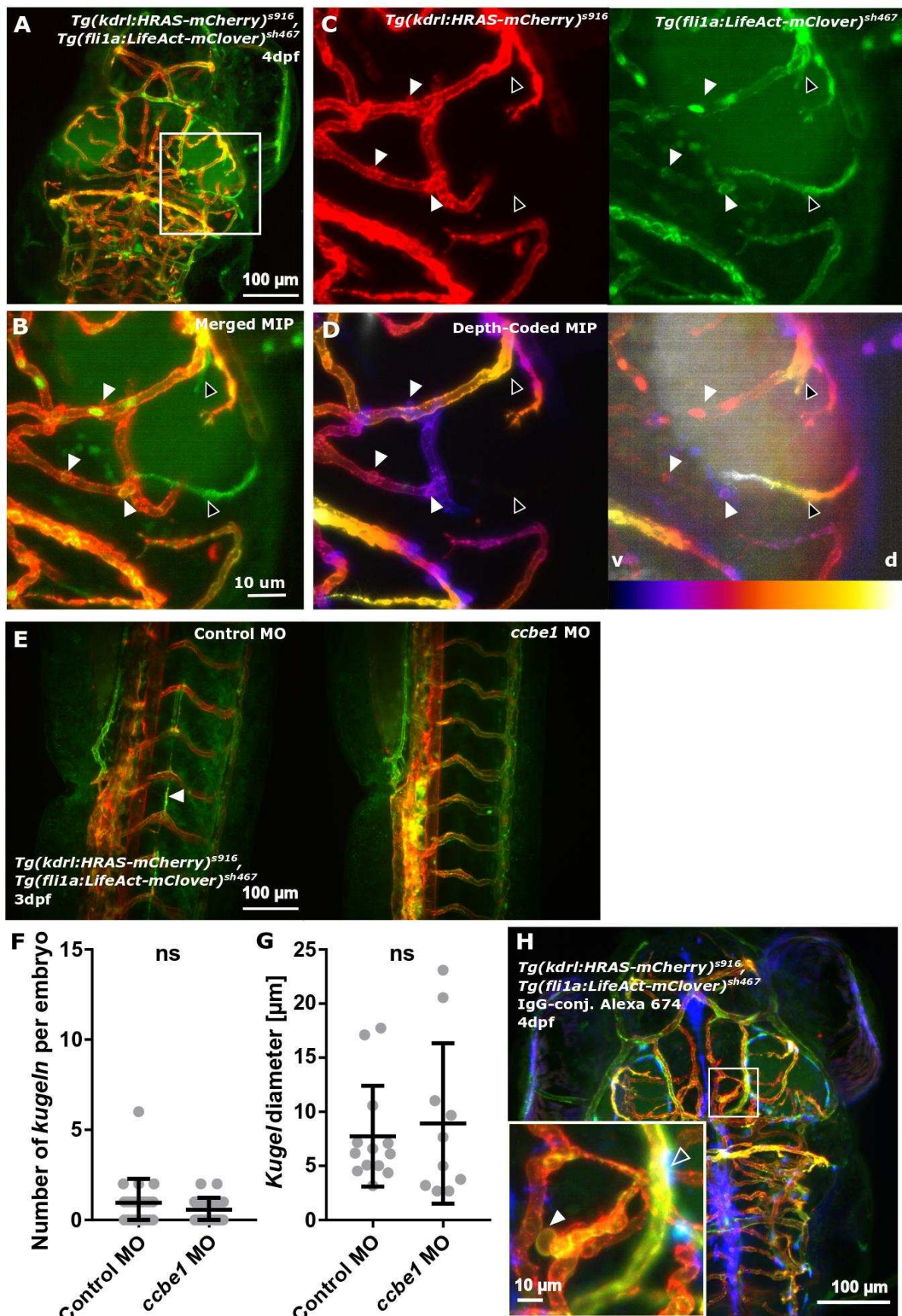


Figure 5| Kugeln do not interact with brain lymphatic endothelial cells (BLECs) in *Tg(fli1a:LifeAct-mClover)*^{sh467}, *Tg(kdrl:HRAS-mCherry)*^{s916}, nor do they take up injected IgG-conjugated Alexa 674.

A Kugeln were studied in the double-transgenic *Tg(fli1a:LifeAct-mClover)*^{sh467}, *Tg(kdrl:HRAS-mCherry)*^{s916}.

B BLECs were mClover positive and mCherry-negative (BLECs - black arrowheads; kugeln – white arrowheads).

C No direct physical interaction between kugeln (BLECs - black arrowheads; kugeln – white arrowheads) and BLECs was observed (n=21 4dpf embryos; 3 experimental repeats).

D Depth-coded MIPs showed that BLECs and kugeln are present on different anatomical planes (depths; purple ventral (v), white dorsal (d); BLECs - black arrowheads; kugeln – white arrowheads).

E *Ccbe1* morpholino (MO) injection led to a loss of lymphatics (white arrowhead).

F Kugel number was not statistically significantly altered by *ccbe1* morpholino (MO) knockdown ($p = 0.3496$; control MO n=22 embryos 0.95 ± 0.28 (mean \pm s.e.m.), *ccbe1* MO n=23 embryos 0.57 ± 0.14 (mean \pm s.e.m.); 3dpf; 3 experimental repeats; Mann-Whitney U test).

G Kugel diameter was not statistically significantly altered by *ccbe1* MO knockdown ($p = 0.8783$; control MO n=21 kugeln from 22 embryos 7.75 ± 1.29 (mean \pm s.e.m.), *ccbe1* MO n=13 kugeln from 23 embryos 8.93 ± 2.35 (mean \pm s.e.m.); 3dpf; 3 experimental repeats; Mann-Whitney U test).

H Injection of IgG-conjugated Alexa 647 into the tectum showed no uptake (blue; unfilled arrowhead) by kugeln (white arrowhead; 140 kugeln from 17 4dpf embryos; 2 experimental repeats).

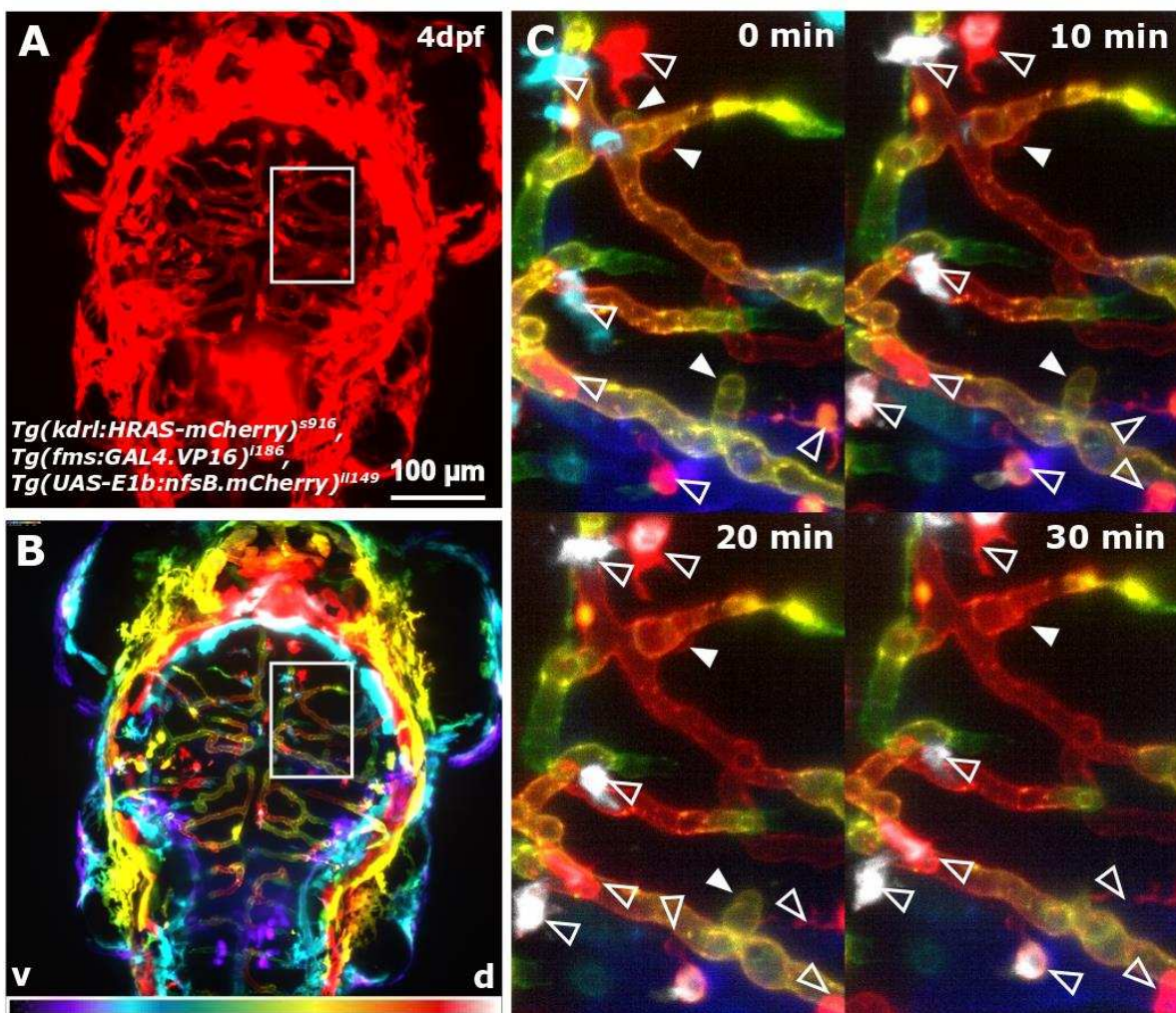


Figure 6| Kugeln do not interact with macrophages.

A The possible interaction of macrophages with kugeln was studied in the transgenic *Tg(kdrl:HRAS-mCherry)^{s916}*, *Tg(fms:GAL4.VP16)ⁱ¹⁸⁶*, *Tg(UAS-E1b:nfsB.mCherry)^{il149}*,

visualizing macrophages and the vasculature simultaneously.

B Coloured depth-coding indicates the different anatomical depths of kugeln and macrophages (ventral purple, dorsal white).

C Maximum intensity projections of z-stacks acquired every 10 minutes during a time-lapse showed no interaction of macrophages (unfilled arrowhead) with kugeln (filled arrowhead; n=21 kugeln in 8 3dpf embryos). Macrophages are all white, indicating they are on a different z-plane to the vessels seen.

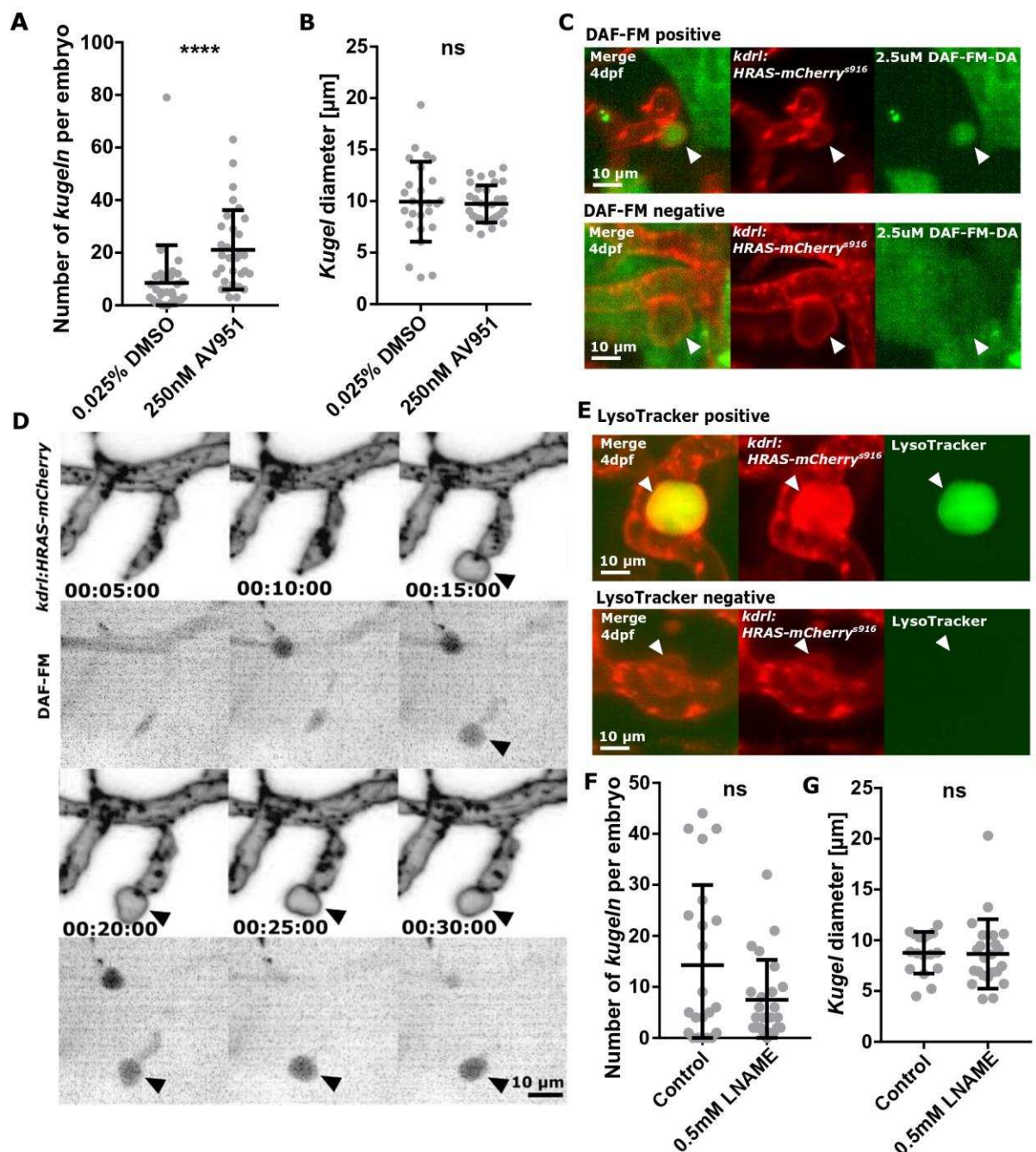


Figure 7| Kugel number is increased by VEGF inhibition, and kugeln contain NO.

A VEGF inhibition by 2h treatment with AV951 statistically significantly increased kugel number (**p<0.0001; DMSO control n=30 embryos 8.53 ± 2.62 (mean ± s.e.m.);

AV951 n=31 embryos 21.10 ± 2.71 (mean \pm s.e.m.); 4dpf; 4 experimental repeats; Mann-Whitney U test).

B Mean kugel diameter was not statistically significantly different after AV951 treatment ($p = 0.7890$; DMSO control n=243 kugeln from 30 embryos 9.94 ± 0.76 (mean \pm s.e.m.); AV951 n=652 kugeln from 31 embryos 9.73 ± 0.32 (mean \pm s.e.m.); 4dpf; 4 experimental repeats; Student's t-test).

C DAF-FM staining, a vital dye for nitric oxide (NO), showed that 57.56% of kugeln were positive for nitric oxide reactivity ($2.5\mu M$ incubation from 96-102hpf; n=22 4dpf embryos; 118 of 205 kugeln filled; 3 experimental repeats). Images show representative “filled” (DAF-FM positive) and “unfilled” (DAF-FM negative) kugeln.

D Time-lapse acquisition with DAF-FM revealed that kugeln contained NO early in their biogenesis (grey LUT; inverted).

E Application of LysoTracker, a vital dye that stains lysosomes or acidic compartments, showed that 17.08% of kugeln contained acidic contents ($8.33\mu M$; 96-101hpf; n=22 4dpf embryos; 62 of 363 kugeln filled; 3 experimental repeats). Images show representative “filled” (Lysotracker positive) and “unfilled” (Lysotracker negative) kugeln.

F The nitric oxide synthase (NOS) inhibitor L-NAME had no statistically significant effect on kugel number per embryo ($0.5mM$ L-NAME 18h; $p = 0.4870$; control n=22 embryos 14.27 ± 3.35 (mean \pm s.e.m.), L-NAME n=24 embryos 7.46 ± 1.61 (mean \pm s.e.m.); 4dpf; 3 experimental repeats; Mann-Whitney U test).

G Diameter of kugeln was not affected by L-NAME ($p = 0.4161$; control n=315 kugeln from 22 embryos 8.77 ± 0.49 (mean \pm s.e.m.), L-NAME n=179 kugeln from 24 8.66 ± 0.71 (mean \pm s.e.m.); 4dpf; 3 experimental repeats; Mann-Whitney U test).

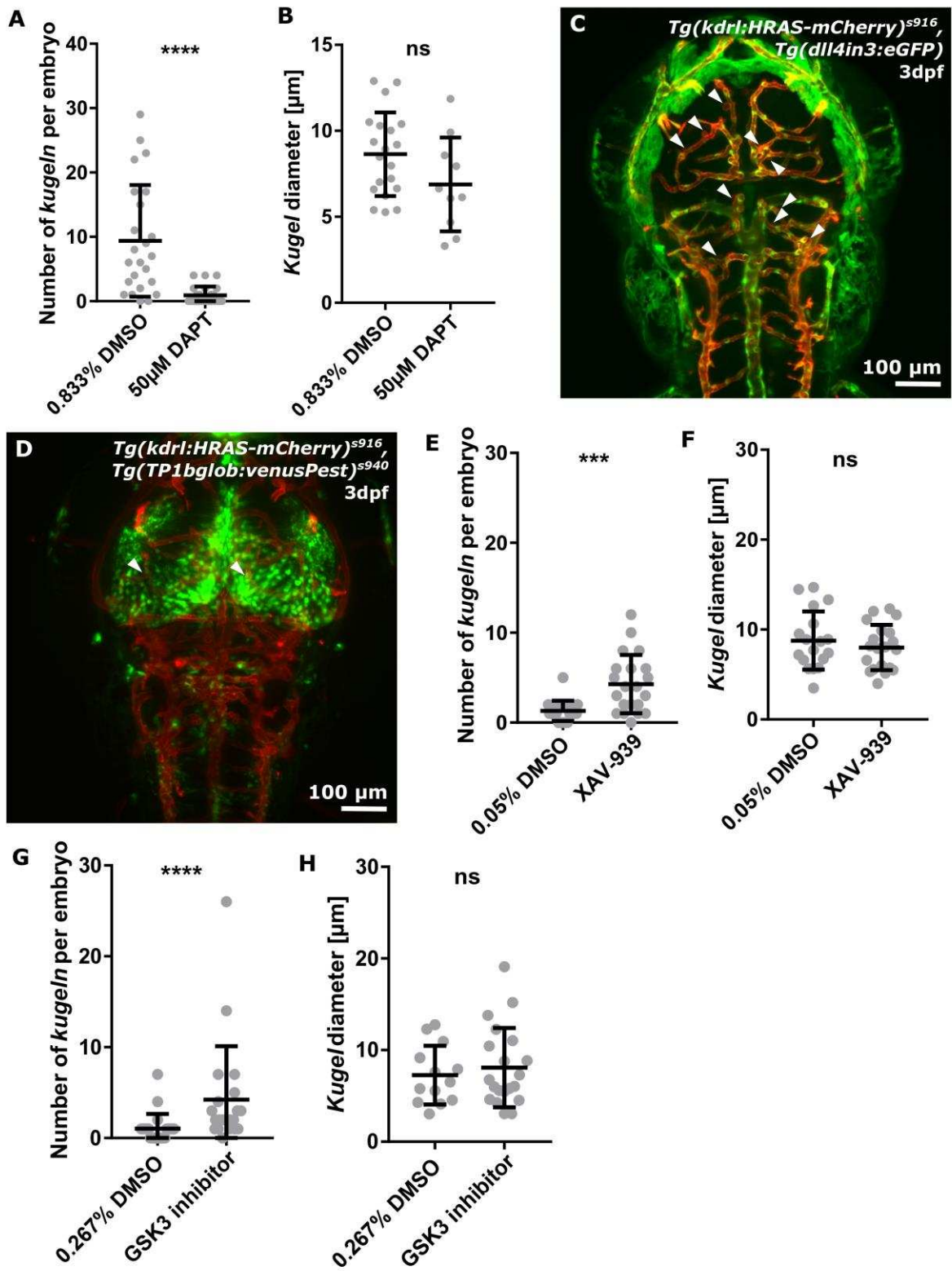


Figure 8| Kugel number is decreased by Notch inhibition but increased by Wnt inhibition or activation.

A Kugel number was significantly decreased by inhibition of Notch signalling by 12h treatment with 50 μ M DAPT (****p<0.0001; control n=24 embryos 9.38 ± 1.77 (mean ± s.e.m.), DAPT n=24 embryos 0.92 ± 0.28 (mean ± s.e.m.); 4dpf; 3 experimental repeats; Mann-Whitney U test).

B Mean kugel diameter was not statistically significantly altered by DAPT treatment (p = 0.0832; control n=225 kugeln from 24 embryos 8.64 ± 0.54 (mean ± s.e.m.); DAPT n=22 kugeln from 24 embryos 6.88 ± 0.86 (mean ± s.e.m.); 4dpf; 3 experimental repeats; Student's t-test).

C A transgenic dll4 reporter line showed no indication of different dll4 expression at the sites of kugeln (white arrowheads pointing to kugeln; n=122 kugeln from 23 3dpf embryos; 2 experimental repeats).

D Studying Notch signalling in the Notch reporter line Tg(TP1glob:venusPest)^{s940}, showed high Notch levels in the mid-brain, but, again, no difference in expression at the sites of kugeln (n=45 kugeln from 19 4dpf embryos; 2 experimental repeats).

E Kugel number was statistically significantly increased by inhibition of Wnt signalling by 4h treatment with 10 μ m XAV-939 (***p = 0.0003; control n=22 embryos 1.32 ± 0.24 (mean ± s.e.m.); XAV-939 n=21 embryos 4.29 ± 0.71 (mean ± s.e.m.); 3dpf; 3 experimental repeats; Mann-Whitney U test).

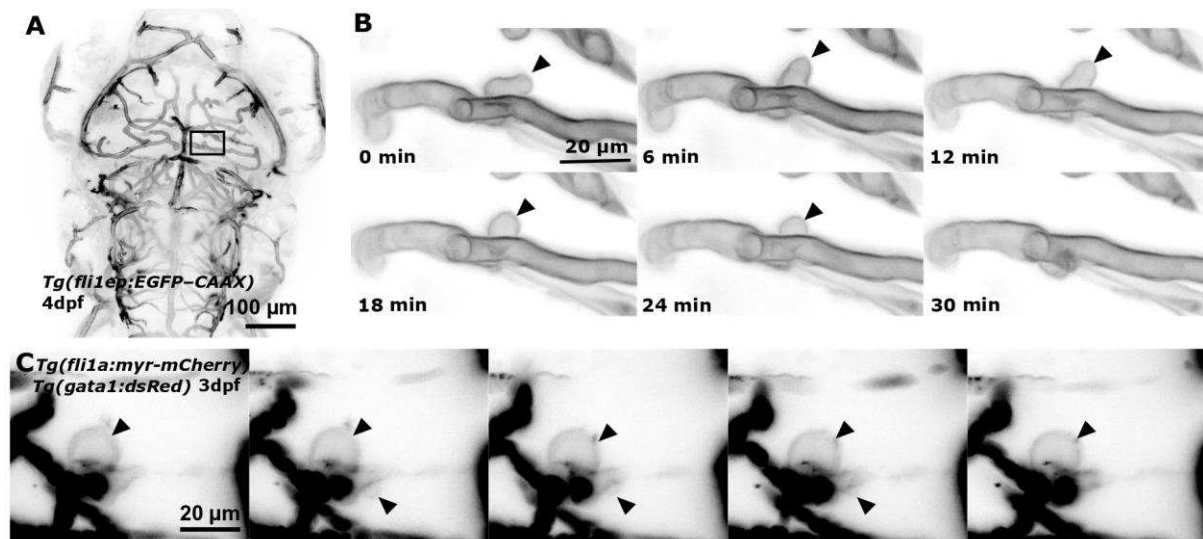
F Kugel diameter was not statistically significantly altered by XAV-939 (p = 0.4098; control n=29 kugeln from 22 embryos 8.78 ± 0.76 (mean ± s.e.m.); XAV-939 n=90 kugeln from 21 embryos 7.99 ± 0.56 (mean ± s.e.m.); 3dpf; 3 experimental repeats; Student's t-test)

G Kugel number was statistically significantly increased by activation of Wnt signalling by 4h treatment with 10 μ m GSK3 inhibition XV (p 0.0359; control n=22 embryos 1.04

\pm 0.34 (mean \pm s.e.m.); GSK3 inhibitor n=21 embryos 4.24 ± 1.28 (mean \pm s.e.m.); 3dpf; 3 experimental repeats; Mann-Whitney U test).

H The diameter of kugel was not statistically significantly altered by GSK3 inhibition (p 0.5555; control n=23 kugeln from 22 embryos 7.26 ± 0.89 (mean \pm s.e.m.); GSK3 inhibitor n=89 kugeln from 21 embryos 8.09 ± 0.97 (mean \pm s.e.m.); 3dpf; 3 experimental repeats; Student's t-test).

Expanded View Figure Legends



- A** MIP of cerebral vessels of 4dpf *Tg(fli1aep:eGFP-CAAX)* embryo.
- B** Time-lapse acquisitions showed that kugeln were dynamic (black arrowhead) as in *Tg(kdrl:HRAS-mCherry)^{s916}*, showing protrusion, shape changes, oscillation and retraction.
- C** Additional time-lapse acquisitions in the *Tg(fli1a:myr-mCherry)*, *Tg(gata1:dsRed)* showed equally dynamics of kugeln (black arrowhead; images grey LUT; inverted).

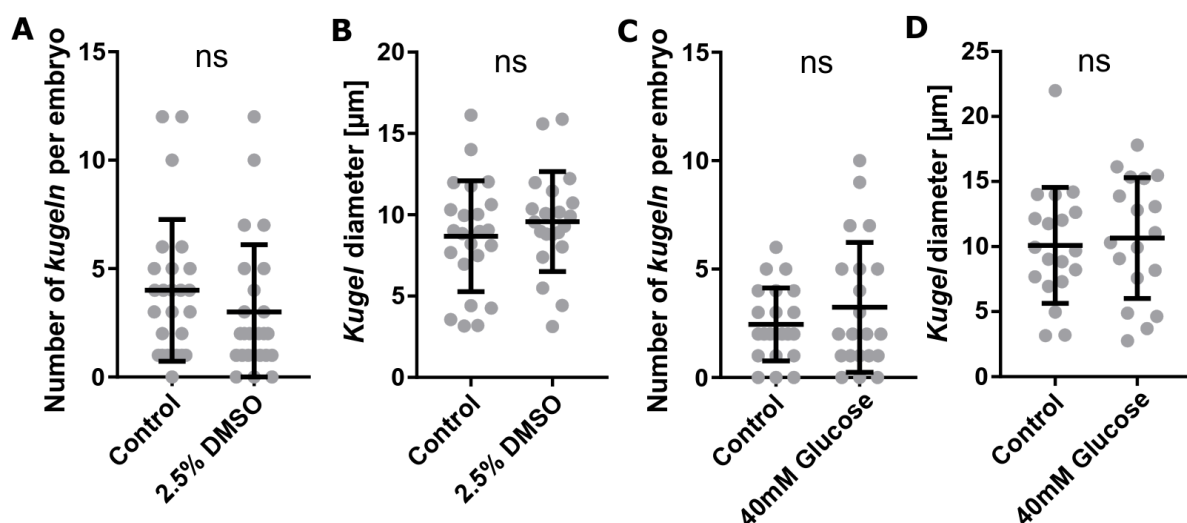


Figure EV 2| Kugeln number or diameter are not altered by changes of membrane permeability or osmotic pressure.

A The influence of membrane permeability increase was studied by application of DMSO; the number of kugeln was not statistically significantly changed (2.5% DMSO 24h; $p = 0.1596$; control n=25 embryos 4.00 ± 0.65 (mean \pm s.e.m.), DMSO n=25 embryos 3.00 ± 0.62 (mean \pm s.e.m.); 4dpf; 3 experimental repeats; Mann-Whitney U test).

B Diameter of kugeln was not statistically significantly different after incubation with DMSO ($p = 0.3665$; control n=97 kugeln from 25 embryos 8.68 ± 0.71 (mean \pm s.e.m.), DMSO n=75 kugeln from 25 9.76 ± 0.67 (mean \pm s.e.m.); 4dpf; 3 experimental repeats; Student's t-test).

C The impact of osmotic pressure on kugeln was studied by application of glucose; no statistically significant difference was observed (40mM glucose 24h; $p = 0.7371$; control n=22 embryos 2.46 ± 0.36 (mean \pm s.e.m.), glucose n=21 embryos 3.24 ± 0.65 (mean \pm s.e.m.); 4dpf; 2 experimental repeats; Mann-Whitney U test).

D Kugel diameter was not statistically significantly different after incubation with glucose ($p = 0.7060$; control n=54 kugeln from 22 embryos 10.09 ± 1.02 (mean \pm s.e.m.), glucose n=67 kugeln from 21 embryos 10.66 ± 4.65 (mean \pm s.e.m.); 4dpf; 2 experimental repeats; Student's t-test).

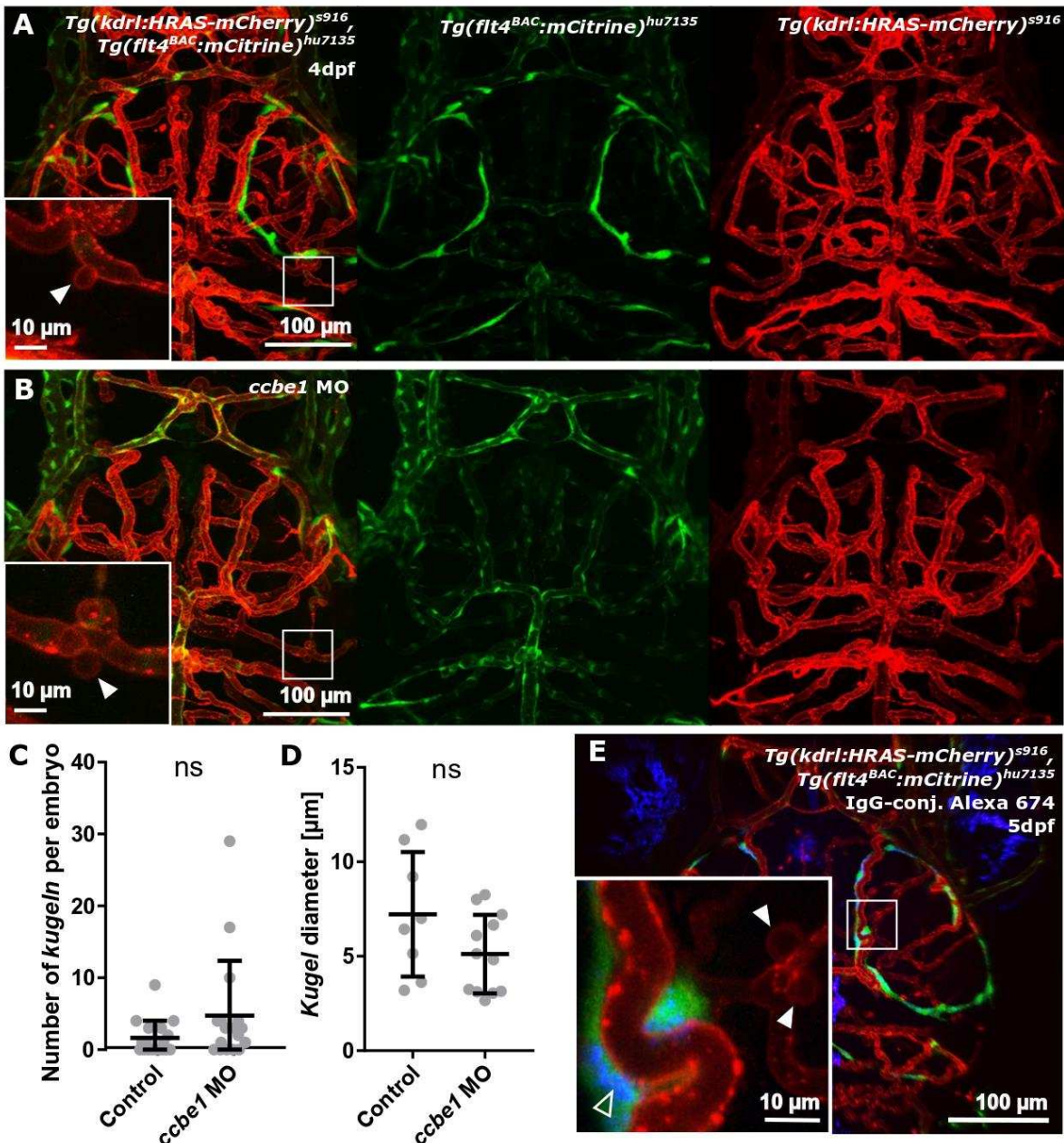


Figure EV 3| Kugeln do not interact with BLECs in *Tg(flt4^{BAC}:mCitrine)^{hu7135}*, *Tg(kdrl:HRAS-mCherry)^{s916}*.

- A** Kugeln (white arrowhead) were additionally studied in the transgenic *Tg(flt4^{BAC}:mCitrine)^{hu7135}*, *Tg(kdrl:HRAS-mCherry)^{s916}*, which was more specific for BLECs, using confocal microscopy to allow higher resolution imaging.
- B** Ccbe1 morpholino (MO) injection lead to loss of BLECs, while kugeln were still observed (white arrowhead).

C The number of kugeln was not statistically significantly altered by *ccbe1* morpholino (MO) knockdown ($p = 0.1472$; control n=17 embryos 1.65 ± 0.58 (mean \pm s.e.m.), *ccbe1* MO n=17 embryos 4.77 ± 1.85 (mean \pm s.e.m.); 4dpf; 2 experimental repeats; Mann-Whitney U test).

D Diameter of kugeln was not statistically significantly altered upon *ccbe1* MO injection ($p = 0.0962$; control n=27 kugeln from 17 embryos 7.22 ± 1.17 (mean \pm s.e.m.), *ccbe1* MO n=81 kugeln from 17 embryos 5.12 ± 0.60 (mean \pm s.e.m.); 2 experimental repeats; Student's t-test).

E Injection of IgG-conjugated Alexa 647 into the tectum (open arrowhead) showed no uptake of IgG-conjugated Alexa 647 by kugeln (n=52 kugeln from 5 5dpf embryos, kugeln indicated by white arrowheads).

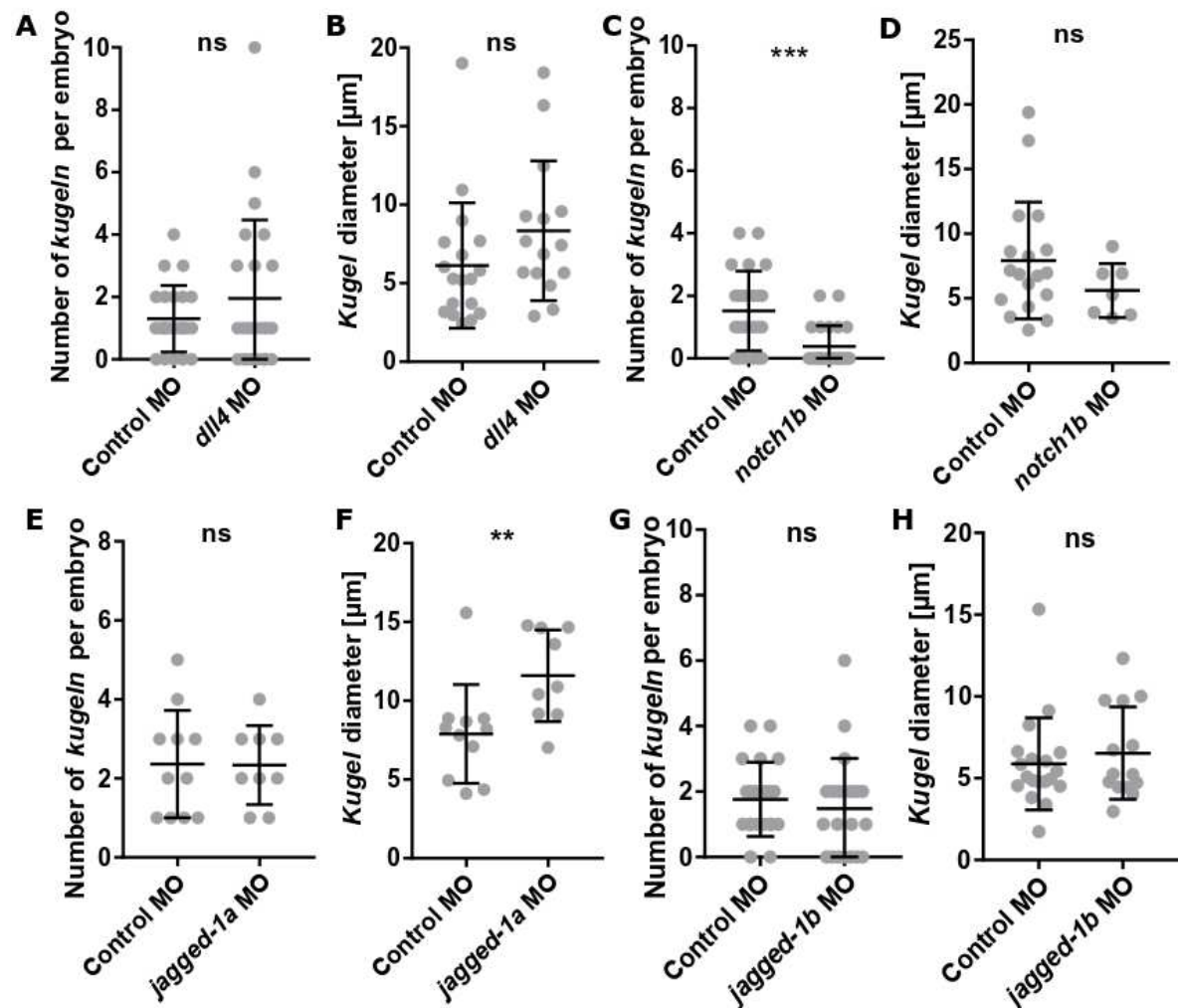


Figure EV 4| The effect of morpholino knockdown of dll4, notch1b, jagged-1a and jagged-1b on kugeln number and diameter.

A Number of kugeln per embryo was not statistically significantly changed upon dll4 MO injection ($p = 0.9639$; control n=23 embryos 1.30 ± 0.22 (mean \pm s.e.m.), dll4 MO n=23 embryos 1.96 ± 0.52 (mean \pm s.e.m.); 3dpf; 3 experimental repeats; Mann-Whitney U test).

B Kugel diameter was not statistically significantly changed upon dll4 MO injection ($p = 0.0843$; control n=30 kugeln from 23 embryos 6.13 ± 0.94 (mean \pm s.e.m.), dll4 MO n=45 kugeln from 23 embryos 8.35 ± 1.15 (mean \pm s.e.m.); 3dpf; 3 experimental repeats; Mann-Whitney U test).

C Number of kugeln was statistically significantly reduced after notch1b MO injection ($***p = 0.0008$; control n=23 embryos 1.52 ± 0.27 (mean \pm s.e.m.), notch1b MO n=23 embryos 0.39 ± 0.14 (mean \pm s.e.m.); 3dpf; 3 experimental repeats; Mann-Whitney U test).

D Kugel diameter was not statistically significantly changed upon notch1b MO injection ($p = 0.3198$; control n=37 kugeln from 23 embryos 7.93 ± 1.07 (mean \pm s.e.m.), notch1b MO n=9 kugeln from 23 embryos 5.61 ± 0.79 (mean \pm s.e.m.); 3 experimental repeats; Mann-Whitney U test).

E Number of kugeln was not statistically significantly changed after jagged-1a MO injection ($p = 0.9563$; control n=11 embryos 2.36 ± 0.41 (mean \pm s.e.m.), jagged-1a MO n=9 embryos 2.33 ± 0.33 (mean \pm s.e.m.); 3dpf; 2 experimental repeats; Student's t-test).

F Kugel diameter was found to be statistically significantly changed upon jagged-1a MO injection ($**p = 0.0097$; control n=23 kugeln from 11 embryos 7.89 ± 0.94 (mean

\pm s.e.m.), jagged-1a MO n=20 kugeln from 9 embryos 11.58 ± 0.97 (mean \pm s.e.m.); 3dpf; 2 experimental repeats; Mann-Whitney U test).

G Number of kugeln per embryo was not statistically significantly changed upon jagged-1b MO injection ($p = 0.3042$; control n=21 embryos 1.76 ± 0.25 (mean \pm s.e.m.), jagged-1b MO n=21 embryos 1.48 ± 0.34 (mean \pm s.e.m.); 3dpf; 3 experimental repeats; Mann-Whitney U test).

H Kugel diameter was not statistically significantly changed upon jagged-1b MO injection ($p = 0.7060$; control n=19 kugeln from 21 embryos 5.88 ± 0.65 (mean \pm s.e.m.), jagged-1b MO n=14 kugeln from 21 embryos 6.53 ± 0.76 (mean \pm s.e.m.); 3dpf; 3 experimental repeats; Mann-Whitney U test).